frontiers in Climate

TYPE Original Research
PUBLISHED 01 July 2026
DOI 10.3389/fclim.2026.1826661

OPEN ACCESS

EDITED BY
Didier Swingedouw,
UMR5805 Environnements et Paléoenvironnements Ocaniques et Continentaux (EPOC), France

REVIEWED BY
Yechul Shin,
Seoul National University, Republic of Korea
Arthur Coquereau,
UMR6523 Laboratoire d'Oceanographie Physique et Spatiale (LOPS), France

*CORRESPONDENCE
Clara Hummel
✉ c.hummel@uit.no;
✉ hummel.cla@gmail.com

RECEIVED 09 March 2026
REVISED 21 May 2026
ACCEPTED 11 June 2026
PUBLISHED 01 July 2026

CITATION
Hummel C, Cotronei A, Myrvoll-Nilsen E, Aksamit N and Rypdal M (2026) Non-linear forcing increases uncertainty in detecting a destabilization of the Atlantic Meridional Overturning Circulation. *Front. Clim.* 8:1826661. doi: 10.3389/fclim.2026.1826661

Non-linear forcing increases uncertainty in detecting a destabilization of the Atlantic Meridional Overturning Circulation

Clara Hummel*, Alessandro Cotronei, Eirik Myrvoll-Nilsen, Nikolas Aksamit and Martin Rypdal

Department of Mathematics and Statistics, UiT The Arctic University of Norway, Tromsø, Norway

The Atlantic Meridional Overturning Circulation (AMOC) plays a critical role in regulating global climate patterns with its potential destabilization and collapse posing significant risks. In this study, we introduce two novel methods to assess AMOC stability, based on a Bayesian framework to estimate its sensitivity, and ensembles of parabolic approximations, respectively. They provide alternative indicators to detect early warning signals (EWSs) for a potential destabilization. By incorporating non-linear and physically motivated drivers, such as temperature and Greenland meltwater runoff, we obtain a more realistic representation of AMOC dynamics and address an important limitation of previous studies, which often rely on linear forcing assumptions. We detect significant EWS for a potential ongoing AMOC destabilization in our sensitivity-based indicator across many combinations of forcing scenarios and response models. However, it revealed large variations, dependent on the considered forcing scenario and methodological choices. While an AR(1) response to linear forcing, consistent with assumptions in previous EWS analyses of the AMOC, emerged as the "best" fit based on Bayes factor analysis, other evaluation criteria provided no clear support. Even though the second EWS indicator, obtained using parabolic approximations, revealed a recent significant peak under linear forcing, and appears to suggest that the AMOC might have passed a critical transition in the late 20th century assuming a temperature driver, we find no clear indication of a considerable destabilization in either case. Our findings highlight the sensitivity of AMOC stability assessments to assumptions about forcing scenarios, response models, and evaluation criteria, emphasizing the need for careful interpretation of EWSs for abrupt transitions in the Earth's climate. While our methods advance EWS analyses by incorporating non-linear forcing and alternative response functions to better represent AMOC dynamics, they also underscore the limitations of applying such tools to complex climate subsystems, represented by one-dimensional time series.

KEYWORDS
AMOC, Bayesian model, critical slowing down, early warning signals, non-linear forcing, sensitivity, stability, tipping points

1 Introduction

The Atlantic Meridional Overturning Circulation (AMOC) is a critical component of the Earth's climate system, responsible for the large-scale transport of heat and salinity across the Atlantic Ocean (Rahmstorf, 1995; Buckley and Marshall, 2016). Its stability is vital for maintaining global climate patterns, as disruptions to the AMOC could have severe impacts worldwide (Stouffer et al., 2006; Drijfhout, 2015; Jackson et al., 2015; Liu et al., 2020). The AMOC is widely regarded as a bistable system, capable of existing in two distinct states: a strong circulation mode, which is currently dominant, and a weak mode. Bistability of the AMOC has first been indicated by hystereses in conceptual box models (Stommel, 1961), which was later confirmed by studies of increasingly complex climate models, spanning Earth system models of intermediate complexity (EMICs, Manabe and Stouffer, 1988; Rahmstorf et al., 2005), coupled atmosphere' ocean general circulation models (AOGCMs, Hawkins et al., 2011) and, more recently, state-of-the-art Earth system models (ESMs, Liu et al., 2017; Romanou et al., 2023; van Westen et al., 2024; Oh et al., 2025). Transitions between AMOC states have further been associated with past abrupt climate changes, such as the Dansgaard-Oeschger (DO) events during the last glacial period (see e.g., Lynch-Stieglitz, 2017). These events, characterized by rapid temperature increases of 5 to 16.5 °C (Kindler et al., 2014), have been considered archetypes of abrupt climate changes (Boers et al., 2022) and have been linked to transitions between weak and strong AMOC modes by multiple lines of evidence (Rahmstorf, 2002; Henry et al., 2016; Boers et al., 2018), underscoring the AMOC's role as a potential key tipping element in the Earth system (Lenton et al., 2008; Armstrong McKay et al., 2022; Boers et al., 2022).

Tipping points (TPs) are critical thresholds, where small perturbations can lead to abrupt and often irreversible changes in a system's state. Systems that exhibit tipping points are often referred to as tipping elements (TEs), which are components of the Earth system that can shift between alternative stable states due to non-linear feedback mechanisms (Lenton et al., 2008). Examples of TEs include the AMOC, the Greenland Ice Sheet (GrIS), and the Amazon rainforest (Lenton et al., 2008; Boers et al., 2022). These systems are particularly sensitive to external forcing, such as changes in temperature or freshwater input, and their transitions can have cascading effects on other components of the Earth system (Lenton et al., 2008; Jackson et al., 2015; Weijer et al., 2019; Gong et al., 2022; Wunderling et al., 2023, 2024).

The AMOC is influenced by a variety of drivers, including changes in freshwater input from the melting Greenland ice sheet, precipitation patterns, and river discharge, which can alter the salinity and density of surface waters in the North Atlantic (Rahmstorf, 1995; Hawkins et al., 2011; Weijer et al., 2019; Gong et al., 2022). These drivers are strongly affected by anthropogenic greenhouse gas emissions and rising global temperatures, which in themselves also play a role, as thermal expansion and increased stratification of the ocean can weaken the AMOC (Liu et al., 2017).

The interplay between these factors is highly complex, and their combined effects can push the AMOC toward a critical threshold, beyond which the system may transition to a weaker state (Stommel, 1961; Lenton et al., 2008; Ditlevsen and Ditlevsen, 2023).

Critical transitions in complex systems like the AMOC are often preceded by characteristic changes in system dynamics, potentially leading to observable changes in quantitative indicators, so-called early warning signals (EWSs). As a system approaches a TP, it becomes more sensitive to perturbations and its ability to recover from them diminishes, which is a phenomenon known as critical slowing down (CSD) (Dakos et al., 2008; Scheffer et al., 2009; Boers and Rypdal, 2021; Lenton, 2011). Most commonly used EWSs are based on CSD and these signals typically manifest as increases in variance and autocorrelation in time series data (Dakos et al., 2008; Scheffer et al., 2009; Boers, 2021). More details on the mathematical background behind such EWS are given in Section 2. Recent studies have identified EWSs in both observational data and model simulations of the AMOC, providing indications for its ongoing destabilization (Boers, 2021; Michel et al., 2022; Ditlevsen and Ditlevsen, 2023; Ben-Yami et al., 2023; Hallali et al., 2025).

Despite these advances, significant uncertainties remain in predicting the timing and likelihood of an AMOC collapse. Challenges include biases in climate models, uncertainties in the representation of external forcing (e.g., freshwater fluxes), and the influence of non-stationary noise on EWS detection. For instance, Ben-Yami et al. (2023) found that uncertainties and pre-processing of observational datasets can lead to biases in CSD analyses. Additionally, Ben-Yami et al. (2024) highlight the limitations of using historical data to robustly extrapolate tipping times, emphasizing the need for robust statistical methods to account for uncertainties in observational datasets and model assumptions. It has further been demonstrated that CSD-based EWS can yield false positives, as they could be detected in model simulations of climate sub-system, such as the AMOC, that don't approach a TP (e.g., Wagner and Eisenman, 2015; Rietkerk et al., 2025; Zimmerman et al., 2025). Moreover, the AMOC's bistability has not been identified in all state-of-the-art Earth system models, raising questions about whether this reflects excessive model stability or a monostable AMOC under current climate conditions (Valdes, 2011; Liu et al., 2014, 2017). Recent studies suggest that high spatial resolution and improved representations of freshwater forcing are necessary to accurately capture the AMOC's response to external perturbations (Drijfhout et al., 2011; Hawkins et al., 2011; Roberts et al., 2013; Liu et al., 2017; Mecking et al., 2017).

A major limitation of many previous studies is the implicit assumption of a slow and linear increase in the forcing parameter when detecting EWSs based on CSD. However, the temporal evolution of the forcing parameter often shows a non-linear dependence on time, and is influenced by complex interactions between external drivers. The assumption of a linear driver can be problematic because it doesn't allow to distinguish whether the AMOC, or any other TE under investigation, destabilizes as a response to linear forcing or whether it responds linearly to a non-linear change in the forcing. As a result, this assumption can lead to a biased detection of CSD. Hallali et al. (2025) address this limitation by incorporating the temporal evolution of freshwater forcing from Greenland melt water directly into their Bayesian framework and further eliminate the need for moving time windows, which are typically used in EWS analyses.

Here, we introduce two new methods to detect changes in a system's sensitivity while taking the temporal evolution of potential forcing parameters into account and apply them to AMOC fingerprint data, where we consider Greenland meltwater runoff, Northern hemisphere temperatures, linear and random forcing (see Section 3.1). Although our methods rely on estimates in moving time windows, we focus on evaluating all possible combinations of window lengths and locations, and examine the consistency of results across these choices.

Our first method, Running Maximum Likelihood Approximation (RMLA, Section 3.2) uses a Bayesian modeling framework to approximate the AMOC's response to a given forcing in moving time windows. These approximations yield estimates of the system's sensitivity, where an increase can be seen as EWS. This approach is largely based on Rypdal et al. (2018), where equilibrium climate sensitivity is inferred from radiative forcing and global temperature. Previous CSD-based EWS analyses of the AMOC (Boers, 2021; Michel et al., 2022; Ditlevsen and Ditlevsen, 2023; Ben-Yami et al., 2024; Hallali et al., 2025) (implicitly) assume that the AMOC can be (locally) approximated by an autoregressive process (see Sections 2 and 3.2). While we also consider such autoregressive approximations, we further include representations as fractional Gaussian noise (fGn) processes, which allow to capture long-range dependent stochastic properties more accurately (Mandelbrot and Van Ness, 1968). Estimations of correlation times related to fGn processes, notably the local Hurst exponent H, have previously been used as EWS (Rypdal, 2016; Boers, 2018; Hummel et al., 2025). It has further been demonstrated by Mei et al. (2023) that local Hurst exponents might offer greater robustness against spurious external signals compared to indicators based on variance and lag-one autocorrelation in folded bifurcation models. This flexibility of applying different statistical models within our framework allows for a more comprehensive analysis of the system's stability and its response to external forcing, providing a more robust framework for detecting early signs of destabilization.

Our second approach, the PARCAD method (Section 3.3) is based on multiple parabolic approximations of the AMOC as a function of values of the forcing parameter, namely Greenland meltwater runoff, Northern hemisphere temperatures, and linear forcing. Polynomial, in particular parabolic, approximations have previously been used to anticipate abrupt transitions (Ditlevsen and Ditlevsen, 2023). However, their reliability in approximating critical thresholds and underlying stable branches of climate subsystems, such as the AMOC, remains debated (Ben-Yami et al., 2024; Cotronei et al., 2026). Instead of relying on individual approximations to estimate a critical threshold, we therefore consider families of approximations on varying intervals to gain insight into whether the AMOC might be approaching a TP. This further allows us to determine whether AMOC proxy data could approximate a stable branch of an underlaying dynamical system (see Sections 2 and 3.3), in which case nearby intervals yield consistent threshold estimates.

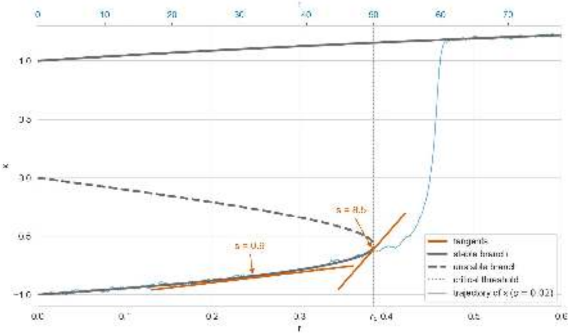

FIGURE 1
System with a saddle-node bifurcation. Bifurcation diagram (gray) with stable (solid lines) and unstable (dashed line) equilibria x^*, as well as example trajectory (blue) of $dx(t) = [-x^3 + x + r(t)]dt + \sigma dB(t)$, where $r(t) = r_c\ t/50$, such that the critical point $r_c = 2\sqrt{3}/9$ (dotted vertical gray line) is reached at $t = 50$. Example values of the sensitivity s are illustrated as the slope of the tangents (orange lines) of the lower stable branch at two different forcing levels r.

2 Mathematical background

In this study, unless specified otherwise, we hypothesize that the system under investigation conforms to the established theoretical framework frequently employed for CSD-based EWSs as used by e.g., Boers (2018); Boers and Rypdal (2021); Ditlevsen and Ditlevsen (2023); Dakos et al. (2008); Ashwin et al. (2012); Boers (2021); Ben-Yami et al. (2024); Myrvoll-Nilsen et al. (2025); Hummel et al. (2025). While this might be an oversimplification for many real climate subsystems like the AMOC, we assume that it can be modeled by a first-order stochastic differential equation (SDE) of the form

$$dx(t) = \big(f(x) + r\big)\, dt + \sigma\, dB(t), \tag{1}$$

where x is a scalar variable representing the state of the system, $dB(t)$ represents a white noise, and r is the driving control parameter, or forcing, of the system. In most previous analyses of EWSs, it is generally assumed that r evolves slowly and linearly with time (Witelski and Bowen, 2015). If $f(x)$ is a non-linear function and if the number of zeros of $f(x) + r$ changes with r, the system in Equation 1 might undergo a fold bifurcation at a critical point r_c (Strogatz, 2018), which represents the "archetype" of bifurcation-induced tipping. An example of such a system is depicted in Figure 1, where $f(x) = -x^3 + x$. Further details on this system can be found in Section 1.4 of Supplementary material.

It is further assumed that the system state x fluctuates around a stable fixed point $x^* = f^{-1}(-r)$. The equilibrium sensitivity s of x with respect to r can then be defined as

$$s = \frac{dx^*}{dr}. \tag{2}$$

As such, it describes how much the system state changes in response to changes in the forcing $r = r(t)$. Figure 1 illustrates that the sensitivity s to forcing r corresponds to the slope of the tangent of the stable equilibrium x^* at r. If the system has a fold bifurcation and approaches the critical point r_c along a stable branch, the equilibrium sensitivity will increase and diverge to infinity as $r \to r_c$.

It should be noted that the critical point r_c of a system does not necessarily coincide with the point where the bifurcation manifests in a given trajectory, i.e., where dx/dr increases steeply. Here, we consider r_c to be the bifurcation point of the underlying system. Due to inertia of a system and the influence of noise, the transition of a trajectory between stable states can occur before or after r_c has been reached, which can also be seen in Figure 1.

The idea behind the commonly used fluctuation-based EWSs is that the statistical properties of these fluctuations change as the control parameter r approaches the critical value r_c. Linearisation around x^* yields a linear SDE, known as the Langevin SDE, for the fluctuations $\Delta x = x - x^*$ around it

$$d\Delta x(t) = -\lambda \Delta x dt + \sigma dB(t). \tag{3}$$

Its solutions define an Ornstein-Uhlenbeck (OU) process with damping parameter

$$\lambda = -f'(x^*).$$

Applying the chain rule, we can see that λ is inversely proportional to the sensitivity s as defined in Equation 2

$$\lambda = \left(\frac{dx^*}{dr}\right)^{-1} = \frac{1}{s}.$$

We further note that the variance of an OU process is proportional to the sensitivity s of the stable equilibrium x^* to the control parameter r:

$$\mathrm{Var}\left(\Delta x(t)\right) = \frac{\sigma^2}{2\lambda} = \frac{\sigma^2}{2}\frac{dx^*}{dr} = \frac{\sigma^2}{2}s. \tag{4}$$

The discrete-time equivalent of an OU process, as defined by Equation 3, is an autoregressive process of order 1 (AR(1) process) with lag-one autocorrelation parameter $\rho = e^{-\lambda}$. Thus, the sensitivity can be expressed in terms of this commonly used EWS by

$$s = \frac{-1}{\log(\rho)}. \tag{5}$$

While the sensitivity s can be related to the commonly used fluctuation-based EWSs of variance and lag-one autocorrelation parameter (Equations 6-7), it is important to mention that its estimation is not purely based on those fluctuations around a stable equilibrium x^*. It further does not require the (implicit) assumption of a slow and linear increase of the forcing parameter r, instead the temporal evolution of $r = r(t)$ can be taken into account. More details on how we obtain estimates of the sensitivity s in this analysis are given in Section 3.2

3 Materials and methods

3.1 Data

As a proxy for the AMOC strength, we use the AMOC fingerprint introduced by Ditlevsen and Ditlevsen (2023), which has further been analyzed by Hallali et al. (2025) and Cotronei et al. (2026), since continuous direct observations only date back to 2004 (Smeed et al., 2014). The fingerprint is constructed from sea surface temperature (SST) anomalies in the subpolar gyre (SPG) region of the North Atlantic, and adjusted by subtracting twice the global mean SST anomaly to account for polar amplification effects under global warming. SST data has been derived from the Hadley Center Sea Ice and Sea Surface Temperature dataset (HadISST) (Rayner et al., 2003) and the seasonal cycle has been removed. The fingerprint is available in monthly resolution and spans the years 1870–2020. To ease computational costs and to match the resolution of all considered forcing scenarios, we use annual means from 1871 to 2020. Similar SPG-based AMOC fingerprints (Caesar et al., 2018; Rahmstorf et al., 2015) are commonly used and have been validated through comparisons with direct AMOC measurements and climate model simulations, demonstrating their utility as a proxy for AMOC strength (Latif et al., 2004; Caesar et al., 2018; Jackson and Wood, 2020). However, their ability to capture stability changes remains debated and modeling studies revealed that such fingerprints may not accurately capture variations of AMOC strength on longer, interdecadal to centennial time scales (Little et al., 2020; Zhu et al., 2023), potentially missing transitions between AMOC states. While alternative AMOC proxies (e.g., based on salinity pile-up in the South Atlantic; Zhu and Liu, 2020; Zhu et al., 2023) exist, we focus our analysis on the SPG-based fingerprint to facilitate comparison with previous EWS and stability analyses of the AMOC.

In order to compare our results with previous EWS analyses of the AMOC, we consider a linear forcing scenario, which corresponds to a linear increase in the time unit, i.e., the years 1871–2020.

To account for a potential freshwater driver of the AMOC, we regard yearly forcing proportional to the cumulative surface melt in Central West Greenland (CWG), which yields a proxy for integrated meltwater runoff. We consider the integrated Central West Greenland surface melt (iCWG) as the cumulative sum over the CWG melt stack derived from ice cores by Trusel et al. (2018), which is available until 2013.

Greenland meltwater runoff contributes to the effective freshwater flux, which is broadly considered as realistic forcing for the AMOC (Rahmstorf et al., 2005; Hofmann and Rahmstorf, 2009). However, other components of the freshwater budget, such as river discharge or changes in precipitation patterns, are not considered in this study.

Furthermore, we employ the annually averaged Northern Hemisphere mean near-surface temperature anomalies relative to 1961–1990 (NH NST) of the Met Office Hadley Center/Climatic Research Unit data set (HADCRUT5.0.2.0) (Morice et al., 2021) as temperature forcing. The resulting temperature anomalies display a relatively high interannual variability, compared to the linear and runoff-based forcing time series. To capture long-term temperature evolution, rather than internal climate variability, we therefore primarily focus our analysis with the PARCAD approach to a smoothed version of NH NST, obtained by applying a Butterworth lowpass filter of order four with a cutoff at 20 years to the annual averages.

Global mean temperature (GMT) has previously been proposed as temperature forcing for AMOC stability analyses (Boers, 2021). Since Northern Hemisphere temperatures are more directly related to freshening of the North Atlantic than GMT, we choose NH NST as a general proxy for anthropogenic global warming instead.

The SPG-based AMOC fingerprint and the different forcing scenarios are depicted in Figure 2.

For the RMLA approach, we additionally consider a random forcing scenario, for which we construct an artificial time series consisting of $n = 150$ independent and identically distributed (iid) samples from a standard normal distribution, denoted as random or iid Gaussian forcing in the following (not shown in Figure 2).

While such random forcing does not represent any known physical driver of the AMOC, and is not used to quantify uncertainty of the method, it provides an alternative to the assumption of a linearly increasing forcing parameter, where forcing mechanisms are unknown or cannot be easily quantified by a single parameter.

We further note that we use normalised forcing for this approach obtained as $(r - \bar{r})/\sigma_r$, where $\bar{r}$ and σ_r denote the mean and standard deviation of the respective forcing time series r.

3.2 Sensitivity changes as EWS—The RMLA method

To capture a variable's sensitivity to a control parameter over time, while accounting for both the system state and the noise evolution, we apply Running Maximum Likelihood Approximation (RMLA). The underlying assumption behind this approach is that a variable's sensitivity to a control parameter can be estimated locally in time by approximating the variable's response by linear response and applying maximum-likelihood methods.

We consider a stationary Gaussian random process of the form

$$x(t) = \int_{-\infty}^{\infty} G(t-s)(r(s)ds + \sigma\, dB(s)), \tag{6}$$

where $G(t)$ is the Green's function to a given deterministic forcing $r(t)$ and random white-noise forcing represented by $dB(t)$. In the following, we denote $X(t) = \int_{-\infty}^{\infty} G(t-s)r(s)ds$ the deterministic term and $Y(t) = \sigma \int_{-\infty}^{\infty} G(t-s)dB(s)$ the stochastic term.

For any Green's function $G(t) = g(t)\Theta(t)$, where $g(t)$ defines the response function, and $\Theta(t)$ is the unit step function, a variable's sensitivity s to changes in the control parameter r can be expressed as

$$s = \int_0^{\infty} g(t)dt. \tag{7}$$

Overall, we follow the approach of Rypdal et al. (2018), which we apply in running windows to obtain a temporal evolution of sensitivity changes. We estimate parameters θ of the response function g of an appropriate form to fit a "simple" model to given data x, forcing r, and (additive) noise structure in moving time windows. As such, this approach allows to capture changes in response and thus sensitivity to linear and non-linear forcing.

While one could consider a wide range of possible Green's functions $G(t) = g(t)\Theta(t)$ in Equation 8, we constrain our choice to two different cases here.

An exponential response $g(t) = e^{-\lambda t}$ yields the integral solution for the linear SDE

$$dx(t) = (-\lambda x(t) + r(t))dt + \sigma\, dB(t). \tag{8}$$

The corresponding stochastic term of Equation 10 describes an OU process, whose discrete-time analogue is an AR(1) process with lag-one autocorrelation parameter $\rho = e^{-\lambda}$. Its sensitivity can be obtained from Equation 9 and is given by

$$s = \int_0^{\infty} e^{-\lambda t}dt = \lim_{t\to\infty} \frac{1}{\lambda}(1 - e^{-\lambda t}) = \frac{1}{\lambda} = \frac{-1}{\log(\rho)}. \tag{9}$$

Using a power law response model $g(t) = \left(\frac{t}{\mu}\right)^{\beta/2-1}$ does not define a SDE. Regardless, the stochastic component of Equation 8, i.e.,

$$Y(t) = \int_{-\infty}^{t} \left(\frac{t-s}{\mu}\right)^{\beta/2-1} dB(s) \tag{10}$$

yields the definition of fractional Gaussian noise (fGn) process (Mandelbrot and Van Ness, 1968) [see appendix of Rypdal and Rypdal (2014)]. It has previously been shown that the corresponding deterministic component yields an accurate description of the Earth's temperature response to known deterministic forcing (Rypdal and Rypdal, 2014; Rypdal et al., 2018). For more details on the motivation behind this approach, see Rypdal and Rypdal (2014) and Rypdal et al. (2018). The parameter β in Equation 12 can be related to the Hurst exponent H associated with fGn by $\beta = 2H - 1$. Local estimates of H in time yield a description of the evolution of correlation times and have been used as EWSs before (Rypdal, 2016; Boers, 2018; Hummel et al., 2025). In this case, the sensitivity diverges $s \to \infty$ reflecting the long-range dependence of the fractional Gaussian noise process.

Using moving time windows, we fit fGn and AR(1) processes with given forcing to each subinterval of the AMOC fingerprint time series, applying a Bayesian modeling framework to obtain time series of the sensitivity estimates s. This is done for window lengths $w = 3, 4, \ldots, n$ years and each window containing w data points centered at their mid-point individually, where n denotes the length of the AMOC and forcing series $x(t)$ and $r(t)$ considered (i.e., $n = 150$ years for linear, temperature and random forcing, and $n = 143$ years for iCWG). To constrain computational costs due to the high number of windows, we perform Bayesian inference using the R package `INLA.climate` (Myrvoll-Nilsen et al., 2020). This approach fits a Bayesian model to obtain posterior marginal distributions $\pi(\theta_j|x)$ of the model parameters $\theta = (\theta_1, \theta_2, \theta_3, \theta_4)$ associated with the fGn and AR(1) process, given the data x and the forcing component r. Thereby computational efficiency is improved in two ways. First, Bayesian inference is obtained using the methodology of integrated nested Laplace approximations (INLA) (Rue et al., 2009, 2017), which provides a computationally superior alternative to traditional Markov chain Monte Carlo (MCMC) methods (Robert and Casella, 1999). Instead of obtaining the posterior distributions by sampling, INLA approximates these using efficient numerical algorithms.

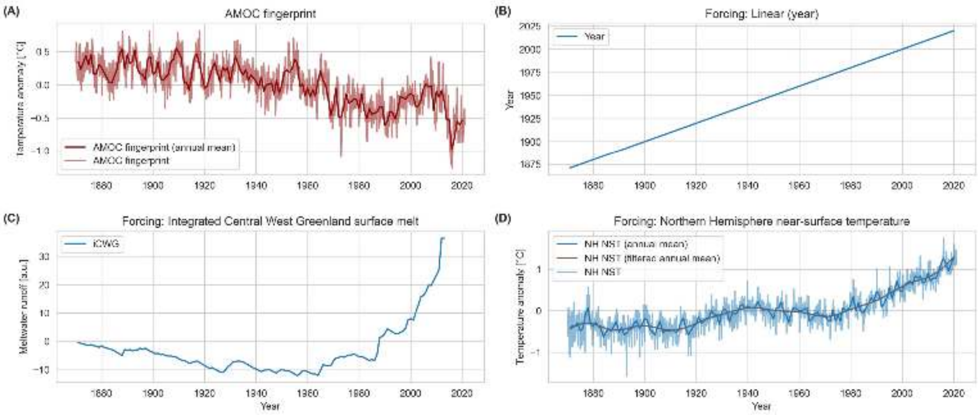

FIGURE 2
AMOC proxy **(A)** and forcing scenarios **(B–D)**. **(A)** Annual mean (dark red) of the AMOC fingerprint as proposed by Ditlevsen and Ditlevsen (2023) (light red) used as system state proxy x. **(B)** Linear trend corresponding to the years 1871–2020 providing linear forcing. **(C)** Integrated Central West Greenland surface melt (iCWG, based on Trusel et al. (2018)) used as proxy for integrated meltwater runoff. **(D)** Northern Hemisphere mean near-surface temperature anomalies (NH NST, light blue) obtained from HADCRUT5 (Morice et al., 2021), its annual mean (dark blue), and filtered annual mean (gray) representing temperature forcing.

Second, the fractional Gaussian noise is approximated using a weighted sum of four AR(1) processes, where the weights b_i and lag-one autocorrelation parameters ρ_i are selected to best reproduce the target autocorrelation function of the fGn process (Sørbye and Rue, 2018, 2019). This reduces the computational time from $\mathcal{O}(n^3)$ to $\mathcal{O}(n)$ and yields very similar results compared to a direct implementation of fGn (Sørbye and Rue, 2018). We note that we use the direct representation (Sørbye and Rue, 2017) to compare how well the different response models and forcing scenarios fit the AMOC data, since the quadruple number of latent variables leads to a biased estimation of the marginal log-likelihood $\log \pi(x)$.

The INLA framework provides posterior marginal means and 95% credible intervals for the parameters θ of the stochastic model, including the autocorrelation parameter ρ and Hurst exponent H of the AR(1) and fGn processes, respectively. For the AR(1) process, we calculate the posterior distributions $\pi(s|x)$ of the sensitivities s by Monte Carlo sampling with $n = 10,000$ samples from the posterior distributions of the autocorrelation parameter $\pi(\rho|x)$ and Equation 11. Using the representation of the fGn model as a superposition of $m = 4$ AR(1) processes, we sample from the posterior distribution $\pi(H|x)$ and use the mapping $\{b_i(H), \rho_i(H)\}_{i=1}^m$ of weights and lag-one autocorrelation parameters to obtain estimates of the sensitivity given by

$$s = s(H) = \sum_{i=1}^{m} \frac{b_i(H)}{-\log(\rho_i(H))}.$$

For a detailed description on how AR(1) and fGn processes are represented within the `INLA.climate` framework, see Myrvoll-Nilsen et al. (2020).

The resulting time series of the mean sensitivity can give an indication whether the AMOC became more or less sensitive to the different forcing evolutions over the given time period and are presented in Section 4.1.2, where we focus on window sizes $w \geq 30$ years. All time series, including shorter windows, can be found in Section 2 of Supplementary material. We note that the parameters ρ and H of the respective processes yield EWS indicators themselves. Time series of their posterior marginal means can be found in Supplementary Figures S6–S9. However, we focus our analysis on the sensitivity of the AMOC.

We note that shorter windows yield longer sensitivity time series and can therefore give more information on recent changes. Nevertheless, those estimates might be uncertain because sensitivity is measured from only few data and forcing values. Longer windows on the other hand might yield more reliable sensitivity estimates, whereas they don't provide information about very recent evolutions.

For each of the tested window lengths $w = 3, 4, \ldots, n$ years, we evaluate whether the resulting sensitivity $s_t = (s_{y_1}, s_{y_2}, \ldots s_{y_n})$ has increased, where $y_1, \ldots, y_n$ represent the years spanned by a given window length w, i.e., the mid-points of the time windows. To do so, we estimate the quantile of the mean sensitivity $\bar{s}_{y_n}$ in the final year y_n within the distribution of sensitivities s_{y_1} in year y_1. Thus, we calculate

$$p = P(\bar{s}_{y_n} > s_{y_1}).$$

We denote an increase to be significant if $p \geq 0.95$. Further, we associate the calculated value of p with the final year y_n of the estimated sensitivities $s_{y_1,\ldots,y_n}$. Figure 3 depicts this procedure and the corresponding results are shown in Section 4.1.2.

3.3 Multiple parabolic approximations—The PARCAD method

As an alternative approach to discern changes in a system's sensitivity to a control parameter, we approximate the time series of the system's state proxy $x_t = x(t)$, where $t = 1, 2, \ldots, n$, by polynomials of order two. In contrast to traditional EWSs for abrupt transitions and our RMLA method, fluctuations around an equilibrium state are not directly taken into account. Given x_t and estimates of the evolution of the control parameter $r_t = r(t)$, $t = 1, \ldots, n$, we fit parabolas

$$P_{a,b}(r) = c_0 + c_1 r + c_2 r^2, \quad r \in \{r_a, \ldots, r_b\} \tag{11}$$

 10.3389/fclim.2026.1826661

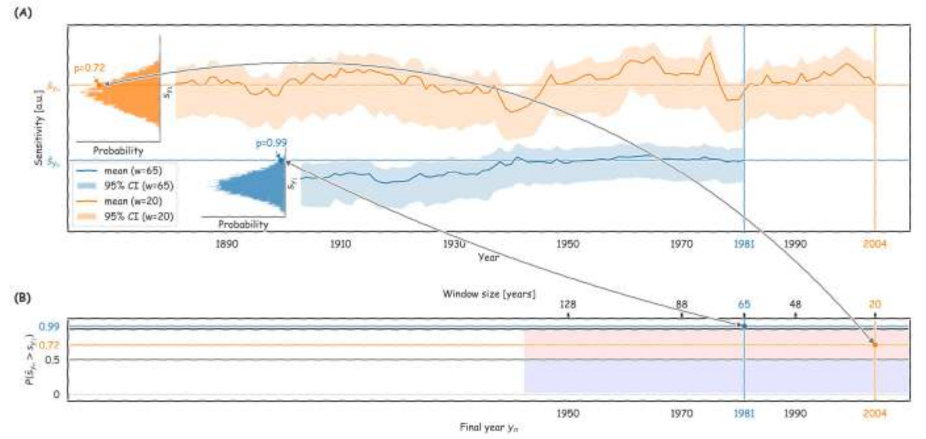

FIGURE 3
Sketch of how the probability of a sensitivity increase is calculated within the RMLA method. **(A)** Example time series of estimated marginal mean sensitivity $\bar{s}$ (bold lines) and corresponding 95% confidence intervals (shaded bands) for two selected window lengths ($w = 65$ years ranging from $y_1 = 1881$ to $y_n = 2004$ in orange, and $w = 20$ years from $y_1 = 1903$ to $y_n = 1981$ in blue). The corresponding marginal distributions of the sensitivity in the first year y_1 of the estimates are shown in the inset histograms. The probability of sensitivity increase $p = P(\bar{s}_{y_n} > s_{y_1})$ is calculated as the quantile of mean sensitivity in the last year $\bar{s}_{y_n}$ within the marginal distribution of s_{y_1} and marked with dots and indicated values of p for each window length. **(B)** Values of p (orange and blue horizontal lines) are associated with the respective final year of estimation y_n for each window size w (vertical lines) and illustrated by the corresponding dots. Red and blue shaded areas indicate increases and decreases of s, i.e., $p > 0.5$ and $p < 0.5$, respectively. The probability of a sensitivity increase is considered significant if $p \geq 0.95$. The thresholds for increasing and significantly increasing sensitivity are shown by gray horizontal lines.

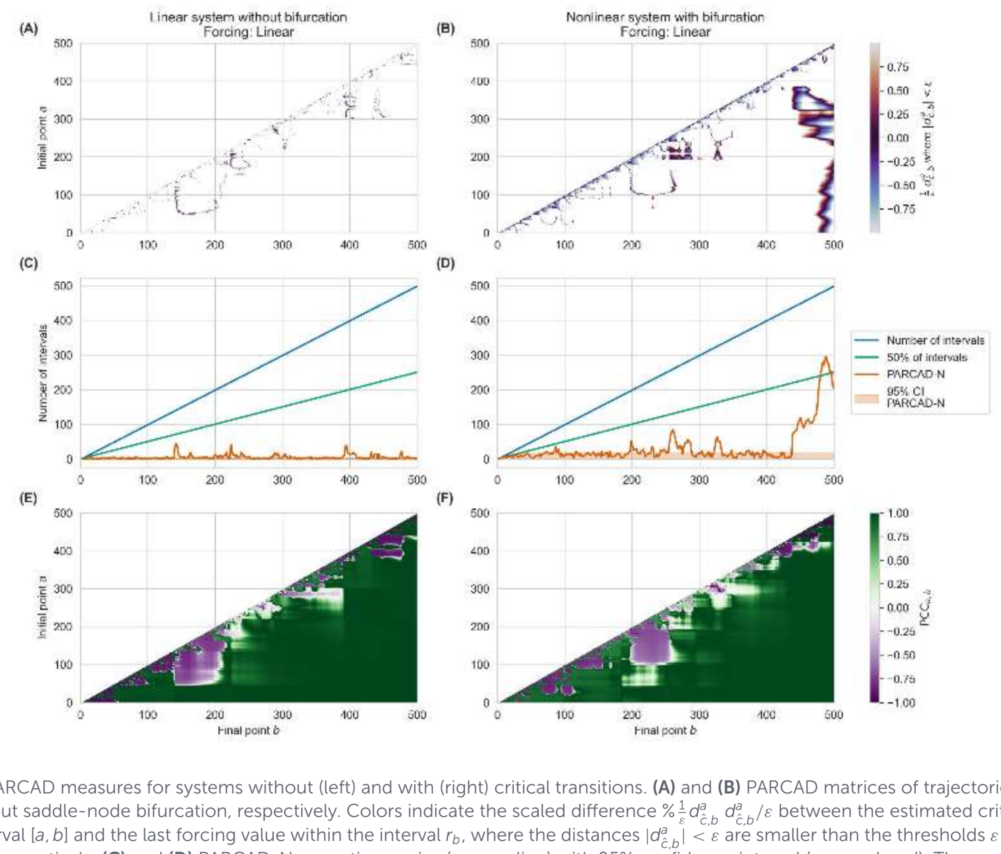

FIGURE 4
Examples of PARCAD measures for systems without (left) and with (right) critical transitions. **(A)** and **(B)** PARCAD matrices of trajectories of systems with and without saddle-node bifurcation, respectively. Colors indicate the scaled difference % $\frac{1}{\varepsilon} d^{a}_{\hat{c},b}$ $d^{a}_{\hat{c},b}/\varepsilon$ between the estimated critical point $\hat{r}^{a,b}_{c}$ within the interval $[a, b]$ and the last forcing value within the interval r_b, where the distances $|d^{a}_{\hat{c},b}| < \varepsilon$ are smaller than the thresholds $\varepsilon = 0.001$ (A) and $\varepsilon = 0.005$ (B), respectively. **(C)** and **(D)** PARCAD-N score time series (orange line) with 95% confidence interval (orange band). The number of possible approximation intervals (blue) represents possible maximum values of PARCAD-N. N score values larger than 50% of intervals (green) are deemed considerable. **(E)** and **(F)** Pearson correlation coefficient PCC$_{a,b}$ between state proxy x_t and its parabolic approximation on $[a, b]$. Both systems are forced by a linear driver and analyzed until the bifurcation point of the non-linear system is reached ($0 \leq r \leq r_c$). Further details and illustrations of the analyzed time series are given in Supplementary material (see Section 1.4, Supplementary Figures S1A, S2A therein).

to the data $A_{a,b} = \{(r_k, x_k) : a \leq k \leq b\}$ using linear regression for all segments $1 \leq a < b \leq n$.

For intervals $[a, b]$ containing at least three unique values, the vertex, or critical point, of each parabola $P_{a,b}(r)$

$$\hat{r}_c^{a,b} = -\frac{c_1}{2c_2} \tag{12}$$

yields an estimate of the critical point r_c of the dynamical system. Considering all possible segments $1 \leq a < b \leq n$, we obtain a family of estimates of r_c using Equation 16.

For systems with a critical transition and increasing control parameter r, many estimation intervals $[a, b]$ preceding and sufficiently close to r_c are expected to yield similar estimates $\hat{r}_c^{a,b}$. In other words, they agree on the presence of an upcoming close transition. Approaching r_c, we further expect those transition estimates to be arbitrarily close to r_b, thus

$$|d^a_{\hat{c},b}| = |\hat{r}_c^{a,b} - r_b| < \varepsilon, \quad \varepsilon > 0. \tag{13}$$

For our analysis of the AMOC, we apply the tolerances ε = 10 years when considering the linear yearly forcing, $\varepsilon = 1$ a.u. for meltwater runoff, and $\varepsilon = 0.1$ °C for NH temperature forcing, in Equations 17–19, respectively. More details on the underlying assumptions, and the choice of threshold parameters ε can be found in Sections 1.1 and 1.2.3 of Supplementary material.

We define the PARabolic Critical Approximation Distance (PARCAD) matrix

$$\text{PARCAD} = [\text{parcad}_{a,b}] = \begin{cases} 1, & r_a < r_b \quad \text{and} \quad |d^a_{\hat{c},b}| < \varepsilon \\ 0, & \text{otherwise} \end{cases}. \tag{14}$$

Since estimation intervals with end point r_b sufficiently close to r_c are expected to yield similar estimates $\hat{r}_c^{a,b}$ close to r_b, we expect to observe vertical patterns of ones in the PARCAD matrix of a system with a critical transition.

For a fixed tolerance $\varepsilon > 0$, we further denote the PARCAD-N score as

$$\text{PARCAD-N} = n_b = \sum_a \text{parcad}_{a,b} = |\{r_a : |d^a_{\hat{c},b}| < \varepsilon\}|. \tag{15}$$

In other words, for each interval end point r_b, we count the number of initial points r_a for which $|d^a_{\hat{c},b}|$ is at most the tolerance. The PARCAD-N score yields an additional measure of the system's non-linearity. If the number of intervals indicating an upcoming transition is close to the total number of points of the time series $x_1, \ldots, x_b$, i.e., the number of possible approximation intervals with end point r_b, we consider a value n_b in PARCAD-N to indicate a potential upcoming transition. As a rough threshold, we require n_b to surpass at least 50% of the number of available points for values in PARCAD-N to be deemed considerable. To further test for significance of PARCAD-N results, we generate 10 000 surrogates by randomly permuting x_t and obtain distributions of n_b values at each time step. We consider a value to be significant if it lies above the 95% confidence interval of the respective surrogate distribution.

As a measure of how well the data is approximated by a parabola within an interval, we calculate the Pearson correlation coefficient between the state space proxy x_t and its parabolic approximations (Equation 15) for all approximation intervals $[a, b]$

$$\text{PCC}_{a,b} = \text{Cor}(x_a, \ldots, x_b; P_{a,b}(r)). \tag{16}$$

We consider high positive values to be an indication that the state space proxy and its parabolic approximation share similar characteristics, particularly the presence of a critical point r_c and increasing sensitivity as r_c is approached.

Examples of PARCAD matrices (Equation 18), the PARCAD-N score (Equation 19) and correlation coefficients (Equation 20) are depicted for a system without critical transition in Figure 4A, D, E, and a system including a critical transition in Figure 4B, D, F, respectively, where the forcing parameter r increases linearly. Further details on the PARCAD method are provided in Section 1 of Supplementary material.

4 Results

4.1 RMLA

4.1.1 Model fit

To compare how well the AR(1) and fGn responses to the different forcing scenarios fit the AMOC data, we calculate the marginal log-likelihood ($\log \pi(x)$, MLIK), deviance information criterion (DIC, Schwarz, 1978; Spiegelhalter et al., 2002), Watanabe-Akaike information criterion (WAIC, Watanabe and Opper, 2010), as well as the log pseudo marginal likelihood (LPML, Ibrahim et al., 2001). The latter is calculated as the logarithmic sum of conditional predictive ordinates (CPO, Pettit, 1990) for each model fit. We note that lower values of DIC and WAIC, as well as higher values of MLIK and LPML indicate a better model fit. The resulting values can be found in Supplementary Table S1. Due to computational reasons, we only consider fits of the entire AMOC time series. The corresponding deterministic responses, as well as exemplary stochastic responses are shown in Figure 5.

While DIC, WAIC, and LPML are comparable between our AR(1) and fGn approximations for each forcing scenario, and the differences between the forcing scenarios are too small to be decisive (see Supplementary Table S1), we observe clear differences between the statistical models considering the marginal log-likelihood.

To interpret the differences in MLIK, we further consider the Bayes factor $B_{i,j} = P(D|M_i)/P(D|M_j)$, where $P(D|M)$ is the marginal likelihood of a model M (i.e., choice of statistical model and forcing scenario), given the (AMOC) data D. Using the obtained marginal log-likelihoods MLIK $= \log(P(D|M))$, we calculate

$$2\log(B_{i,j}) = 2\log(P(D|M_i)) - 2\log(P(D|M_j)),$$

and follow the suggested interpretation of $2\log(B_{i,j})$ by Kass and Raftery (1995), which is depicted in Figure 6.

Figure 6 reveals strong evidence for an AR(1) fit with linear forcing over all other fits, where this evidence can be seen as very strong, when compared to AR(1) responses with random and freshwater forcing. We see a very strong indication against the latter two in comparison to most other response and forcing combinations, with the exception of the fitted fGn response to random forcing, where strong evidence is found. Comparing the different response models for a given

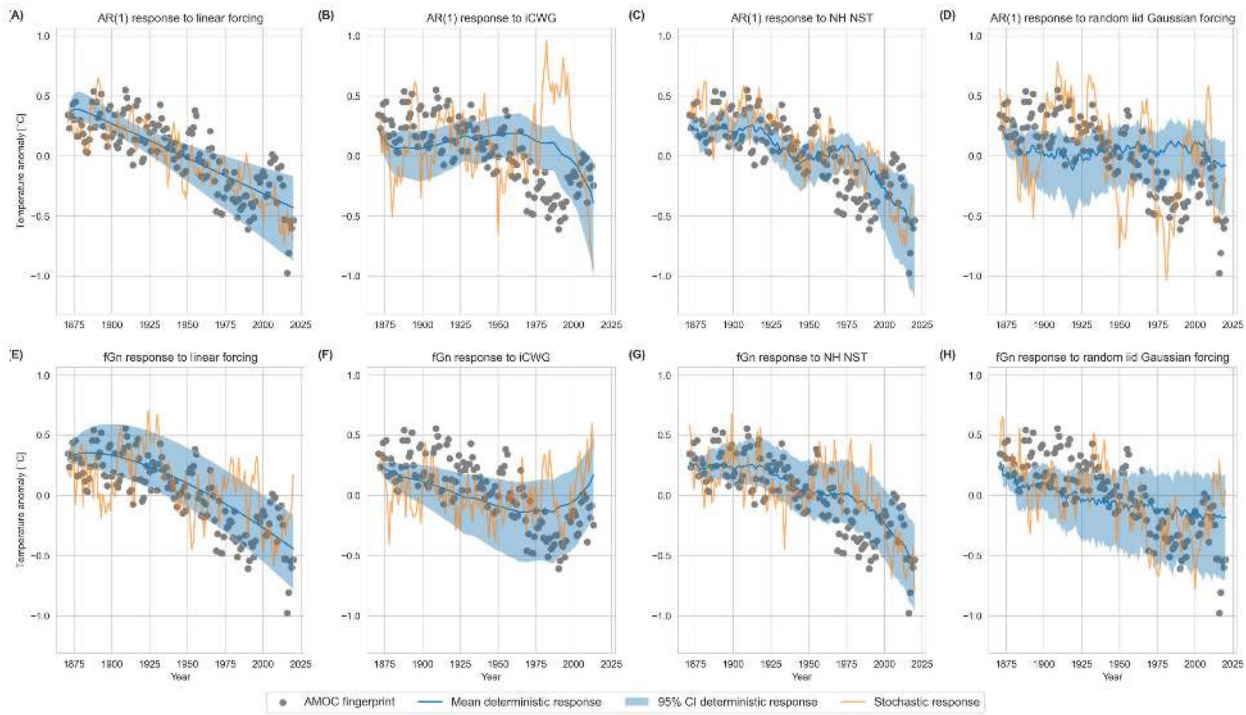

FIGURE 5
RMLE model fits of the AMOC fingerprint, considering AR(1) [top row, **(A–D)**] and fGn responses [bottom row, **(E, F)**] to linear **(A, E)**, meltwater runoff **(B, F)**, temperature **(C, G)** and random forcing **(D, H)**, respectively. The AMOC fingerprint (gray dots) is approximated by the stochastic responses (exemplarily shown in orange) of the maximum likelihood models. Mean deterministic responses with 95% confidence interval are depicted by blue lines and bands, respectively.

forcing, we observe strong indication that an AR(1) model yields a better fit than an fGn process. For freshwater and random forcing, the Bayes factor indicates very strong and strong preference of an fGn response, respectively. Analyses of marginal log-likelohod and the corresponding Bayes factor don't reveal any indication which response fits the AMOC best, when temperature is modeled as the dominant driver. Regardless of response function, our Bayes factor analysis suggests that the "classical" linear forcing scenario seems to best represent the data.

Even though a visual interpretation of how well a model fits might be misleading, we see in Figure 5 that the deterministic responses of the two models with the lowest Bayes factors [AR(1) response to runoff and random forcing, panels (Figure 5B, 5D), respectively] do not align closely with the AMOC fingerprint data. This also applies to the deterministic fGn response to the former (Figure 5F) and to Gaussian noise to a lesser extent [panel Figure 5H]. In those cases, the AMOC variability can be explained by noise to a large degree, whereas it appears to be strongly determined by the AR(1) and fGn responses to linear and temperature forcing scenarios, where their respective deterministic fits closely follow the AMOC data (Figure 5A, C, E, G). Nevertheless, we cannot confirm or deny the viability of a model based on such a visual inspection as a strong influence of noise, or processes not included in our rather simple statistical models, can not be excluded.

4.1.2 AMOC sensitivity

Since sensitivity estimates obtained in short windows might not yield enough data for a reliable sensitivity estimation, we focus this analysis of AMOC sensitivity on longer time scales and omit results for window sizes < 30 years here. This choice is further motivated by the AMOC's intrinsic timescales of multidecadal variability and centennial collapse. Results including all available window lengths ≥ 3 years are depicted in Supplementary Figures S3–S5 in Section 2 of Supplementary material, where results relying on short windows are further described.

The temporal evolutions of the mean AR(1) and fGn sensitivity to the four forcing scenarios (linear, runoff, temperature and random) for all available window lengths ≥ 30 years are depicted in Figures 7, 8, respectively. Regarding the average sensitivity assuming an AR(1) response, we observe increases for comparably short window lengths (ca. 30–50 years) between 1980 and 2000 for all drivers considered. Nevertheless, they appear to be less pronounced for the random forcing scenario. We further observe earlier increases when the model is forced by iCWG for longer windows. The temporal shifts of those might be explained by the use of centered running time windows.

We note the expected sensitivity values observed in the autoregressive processes are generally higher than those for the fGn-based models. Nevertheless, this should not be taken as a sign of increased destabilization, as $s \to \infty$ for a system approaching

10.3389/fclim.2026.1826661

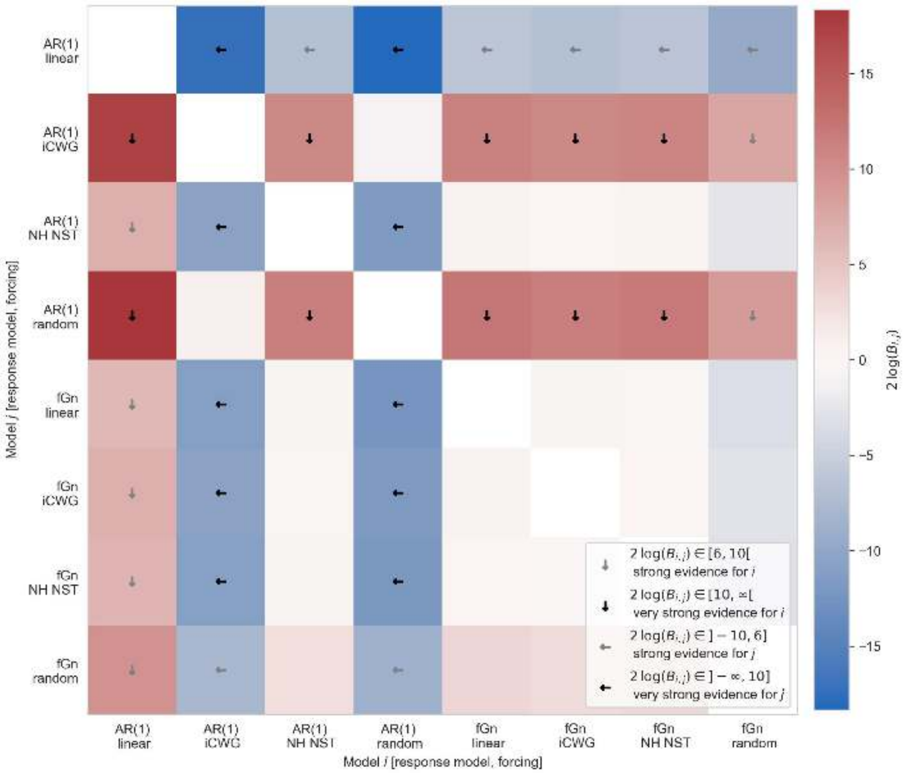

FIGURE 6
Bayes factor analysis of RMLE model fits to the AMOC fingerprint. Colors indicate $2\log(B_{i,j})$ between models i and j, which are specified by their response models (AR(1) and fGn) and forcing time series. (Very) strong evidence for model i is indicated by (black) gray downwards arrows. (Very) strong indication in favour of model j is marked by (black) gray leftwards arrows. Interpretation of logarithmic Bayes factor values follows Kass and Raftery (1995).

a bifurcation. Thus, we are rather interested in (relative) increases of s.

Considering the individual time series of average sensitivity applying an fGn response model (Figure 8), we see increases in all forcing scenarios for most time window sizes. Nevertheless, these seem to occur much earlier than for their AR(1) equivalents described above. Here, the highest (mean) sensitivity is reached in the mid-20th century for very long time windows. Slightly shorter windows, which where seen to peak in the late 20th century assuming an AR(1) response, also peak at this time for all forcing scenarios, with the exception of iCWG, where a decrease following the peak can be seen.

From Figures 7, 8, we see that temporal evolutions of mean sensitivity s vary strongly across forcing scenarios, response models and window size. While these time series can give a first indication on how sensitivity changes over time, and can thus give insight whether the AMOC might be destabilizing, they do not take the entire distribution of s into account. We therefore focus on the probability of an increased sensitivity utilising those distributions as described in Section 3.2 and visualised in Figure 3. They are depicted assuming an AR(1) and fGn response in Figure 9A, B, respectively.

Considering an AR(1) response, we see that there seems to be a significant sensitivity increase for most window lengths, when temperature forcing is considered (Figure 9A). In other words, we observe significantly increased sensitivity between approximately 1955 and 2005. Looking at runoff forcing, using iCWG data, we observe significantly increased sensitivity between approximately 1985 and 1998. sFor random forcing, the same can be observed for most years (and window sizes) between ca. 1995 and 2003. Even though we see an increase in s in later years, this does not appear to be significant. Assuming a linear driver, only very few significant increases have been found, which primarily occur after 2010 and correspond to very short window lengths ($w \leq 20$ years, see Supplementary Figure S3. Furthermore, there are large fluctuations in the probability of an increase in sensitivity, starting in the 1900s. From then on, the probability varies between low to very low values and estimates close to 1 within as little as one year. In other words: by slightly changing window lengths shorter than 60 years by merely a few, in some cases ($w < 40$) just one year, we alternate between detecting a significant increase and observing a decrease in sensitivity. We are thus hesitant to interpret the observed significant sensitivity increases, where linear forcing has been considered, as early warning signals, or indicators of an ongoing destabilization, as they seem to be highly dependent on window size.

Generally, we seem to observe a higher probability of increasing sensitivity using an fGn response than for an AR(1) response, whereas only few window lengths and forcing scenarios yield a decrease in s (Figure 9B).

10.3389/fclim.2026.1826661

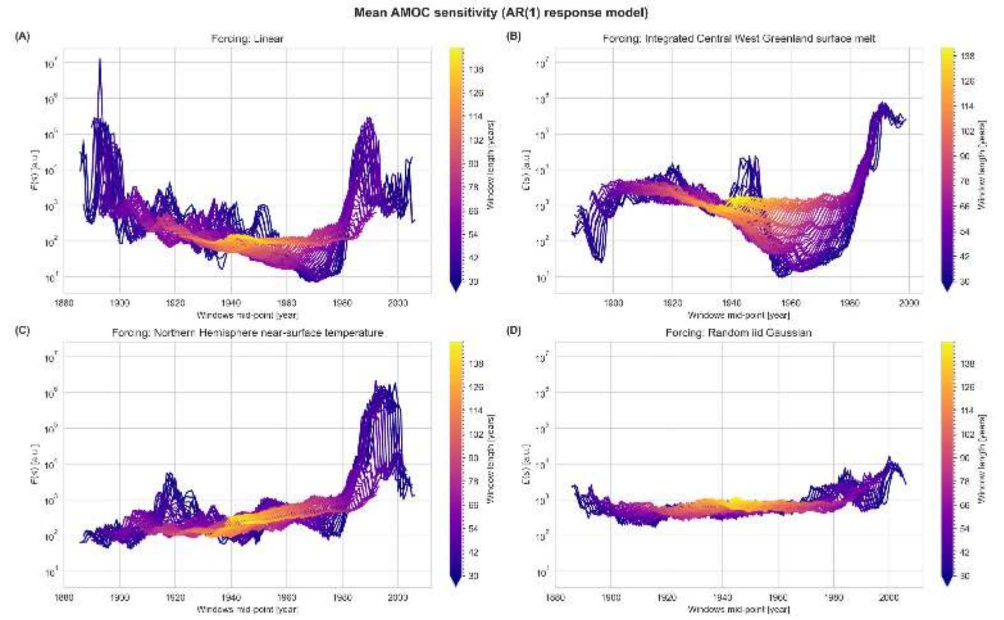

FIGURE 7
Temporal evolution of mean AMOC sensitivity obtained from AR(1) responses to linear **(A)**, meltwater runoff **(B)**, temperature **(C)**, and random forcing **(D)**, respectively, using all available window lengths $w \geq 30$ years (colors). AR(1) models have been fitted within each time window individually to obtain distributions of sensitivity s, whose means $E(s)$ are shown at the windows' mid-point. Note the logarithmic scale of the y-axis.

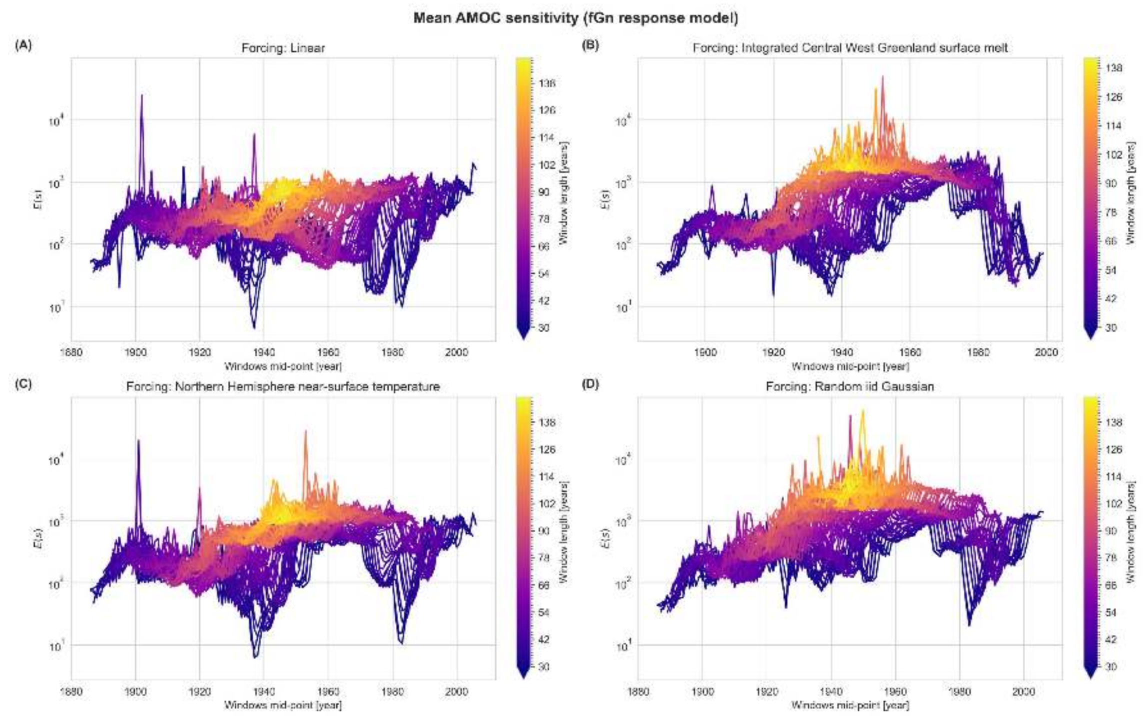

FIGURE 8
Temporal evolution of mean AMOC sensitivity obtained from fGn responses to linear **(A)**, meltwater runoff **(B)**, temperature **(C)**, and random forcing **(D)**, respectively, using all available window lengths $w \geq 30$ years (colors). fGn models have been fitted within each time window individually to obtain distributions of sensitivity s, whose means $E(s)$ are shown at the windows' mid-point. Note the logarithmic scale of the y-axis.

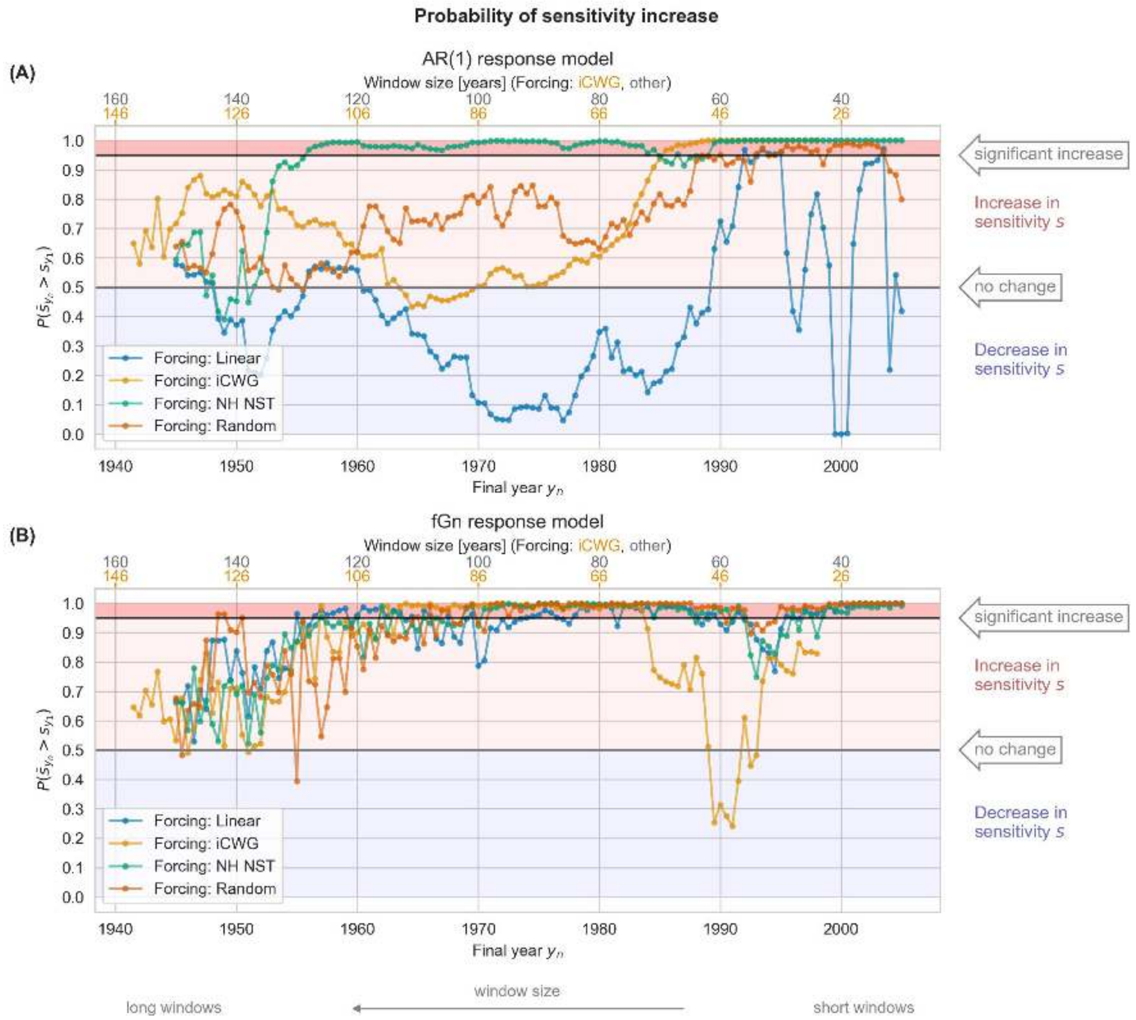

FIGURE 9
Probability of a sensitivity increase considering AR(1) **(A)** and fGn responses **(B)** to linear (blue), meltwater runoff (yellow), temperature (green) and random forcing (red), respectively. The probability $p = P(\bar{s}_{y_n} > s_{y_1})$ is obtained for each window length $w \geq 30$ years and associated with the final year y_n of the corresponding sensitivity estimates, following the scheme shown in Figure 3. Note that for a given final year, window sizes differ between iCWG and other forcing scenarios due to its shorter length. The corresponding window lengths are shown in gray and yellow, respectively. Increases (decreases) of s are indicated by pale red (blue) shaded areas. Significant increases $p \geq 0.95$ are underlaid in red above the significance threshold (black horizontal line).

When considering linear forcing, we see significant sensitivity increases for individual years starting in the 1950s, which are consistently significant between 2000 and 2005. The probability of such an increase remains high and close to the significance level between 1950 and 2005.

For runoff forcing, we observe significantly increases in sensitivity between ca. 1962 and 1983. After this time period, the probability of a sensitivity increase decreases and despite an increase from 1900 is not found to be significant for the time windows ≥ 30 years considered here.

For the temperature forcing scenario, we find this probability to be significant between 1970 and 1987, as well as from 1998 to 2005.

Assuming an fGn response to a random driver, we observe most significant probabilities of increasing sensitivity, notably until 1971 to 1990, and until the time period between 1995 and 2005.

4.2 PARCAD

Applying our method of multiple parabolic approximations, we find little evidence for the proximity of the AMOC to a critical threshold. Looking at the PARCAD matrix for the linear forcing scenario (Figure 10A) we see a vertical pattern toward the end of the AMOC fingerprint time series in the 21st century, similar to the one observed in Figure 4B for a system approaching a critical transition, indicating that the AMOC might approach such a transition. We further see that the corresponding PARCAD-N score (Figure 10D) becomes significant (i.e., exceeds the 95% confidence interval) close to 2020. This indicates that the mean AMOC state seems to change in response to linear forcing. Nevertheless, we note that the PARCAD-N score remains low and not considerable: less than half the considered estimation intervals indicate a close transition. Hence, we do not find

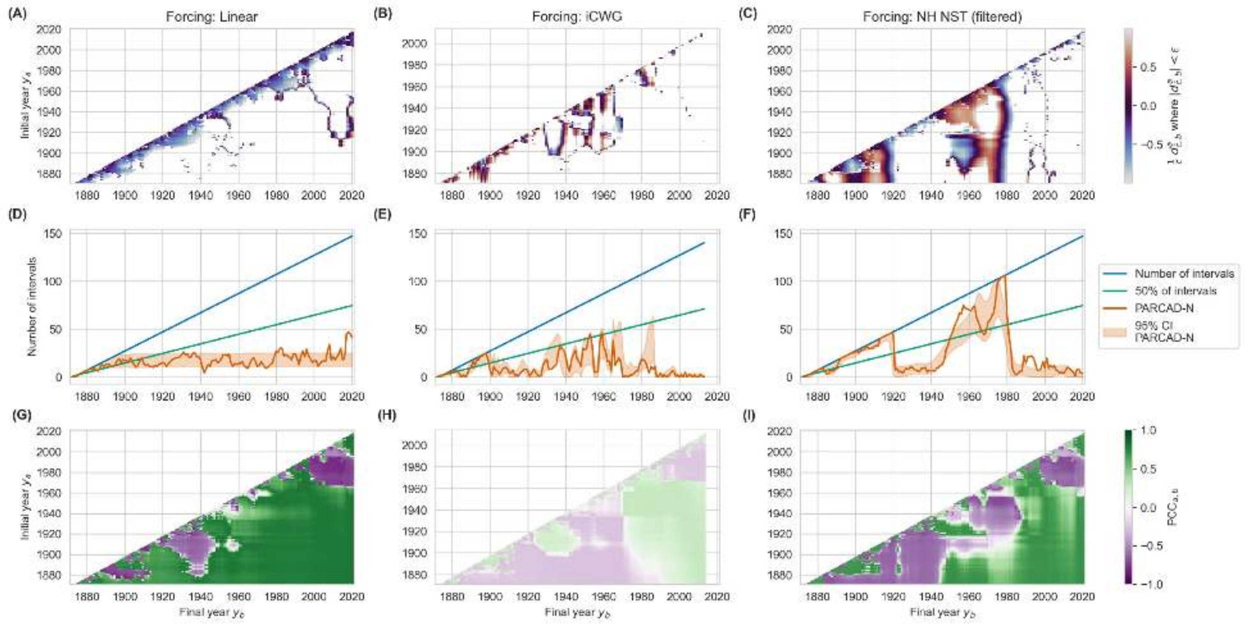

FIGURE 10
PARCAD measures of the AMOC considering linear [left column **(A, D, G)**], meltwater runoff [middle **(B, E, H)**] and filtered temperature forcing [right **(C, F, I)**]. **(A–C)** PARCAD matrices for the different forcing scenarios. Colors indicate the scaled difference $d^a_{\hat{c},b}/\varepsilon$ between the estimated critical point $\hat{r}^{a,b}_c$ within the interval $[a, b]$ and the last forcing value within the interval r_b, where the distances $|d^a_{\hat{c},b}| < \varepsilon$ are smaller than the thresholds $\varepsilon = 10$ years **(A)**, $\varepsilon = 1$ a.u. **(B)**, and $\varepsilon = 0.1$ °C **(C)**, respectively. **(D–F)** PARCAD-N score time series (orange lines) with 95% confidence intervals (orange bands). The number of possible approximation intervals (blue) represents possible maximum values of PARCAD-N. N score values larger than 50% of intervals (green) are deemed considerable. **(G–I)** Pearson correlation coefficients $PCC_{a,b}$ between the AMOC fingerprint and its parabolic approximations on estimation intervals $[a, b]$.

clear indication that the AMOC might be close to a critical threshold.

In contrast to that, we cannot identify similar vertical patterns close to present day in the PARCAD matrix, when Greenland runoff is considered as forcing (Figure 10B). In this case, the PARCAD-N score yields higher values than for linear forcing, where the 50% threshold to be deemed considerable is only marginally exceeded for single years in the 1950s (Figure 10E). Furthermore, we see no significant changes of PARCAD N. This rather indicates that the observed dynamics are externally driven, with little evidence to support the presence of intrinsic system behavior contributing to those changes. Additionally, we observe very low values, close to zero, approaching 2020.

Assuming a temperature driver, however, yields clear vertical patterns in the PARCAD matrix, which are especially pronounced in the 1970s (Figure 10C). We observe steep increases in the N score around 1950, and again, after a decrease in the 1960s, in the 1970s (Figure 10F). This is followed by a sharp decrease in 1980. Toward the end of either increase, we see that this indicator becomes significant. PARCAD-N score values are considerable between 1950 and 1980 and reach their maximal value right before their decrease in 1980. When comparing PARCAD-N to the corresponding correlation coefficients, we see that the peak of N score values coincides with a decrease in $PCC_{a,b}$ during the 1970s. Before and after this time period, the N score remains low and decreases to values close to zero throughout the 21st century. Nevertheless, it was found to be significant between approximately 1990 and 2003.

We note that those results differ greatly when annual means of NH NST are considered, where no filtering has been applied to smoothen the temperature time series. In this case, we cannot identify clear vertical patterns in the PARCAD matrix. Even though the N score can be deemed considerable for many years between 1950 and 1990, it was found to fluctuates a lot. These fluctuations appear to mirror the high interannual variability of NH NST itself. Hence, changes in PARCAD-N might represent internal climate variability and can not be interpreted as a sign of destabilization.

A comparison between PARCAD results using filtered and unfiltered temperature forcing is shown in Supplementary Figure S10 of the Supplementary material.

Moreover, we detect relatively low correlation between the AMOC fingerprint and its parabolic approximations across all cases (Figure 10G–I), particularly for the runoff forcing (where $PCC_{a,b} < 0.3$). While we generally find higher correlation in the linear forcing case than in the non-linear ones, the values remain comparably low and do not exceed 0.8.

This suggests that the given data represents phenomena too complex to be adequately captured by a one-dimensional ODE or parabolic approximations. The low correlation values further highlight the potential need for higher-dimensional models or more sophisticated analytical frameworks to fully capture the intricacies of the AMOC's response to different potential drivers.

5 Discussion

5.1 Key findings

This study introduces two novel methods, RMLA and PARCAD, to assess whether the AMOC might be destabilizing and approaching a potential collapse. These methods incorporate non-linear and physically motivated forcing scenarios, such as Northern Hemisphere temperature and Greenland meltwater runoff, which contrast with the linear forcing assumptions commonly used in previous studies (Boers, 2021; Ben-Yami et al., 2023; Ditlevsen and Ditlevsen, 2023). By explicitly considering non-linear drivers, our approach provides a more flexible, potentially more representative, model of AMOC dynamics and highlights the importance of accounting for the complex interactions between potential drivers, such as atmospheric temperature, freshwater fluxes, and the AMOC.

Using the RMLA method, we found that the linear AR(1) model emerged as the "best" based on Bayes factor analysis. While this might be seen as an indication that classical CSD-based EWSs could provide a valid approach to analyse AMOC destabilization, other evaluation criteria provided no clear support for this conclusion, and alternative response functions or forcing scenarios might yield equally good or better fits.

This underscores the challenge of identifying a "best" or "realistic" model representation. Significant increases in sensitivity s were observed across all forcing scenarios and response models, of which the majority were found after 1970, and in all but one case around the year 2000. These results are in line with multiple independent lines of evidence, from models and observations, for a weakening of the AMOC, characterized by significant changes in AMOC mean state and variability during the late 20th century (Zhu and Liu, 2020; Zhu et al., 2023; Coquereau et al., 2026). However, our results varied substantially depending on the chosen model, forcing, and length of time window. Even though this ensemble of sensitivity estimates yields mixed results when considered as a whole, these findings do not stand in direct contrast to previously found EWSs in observational AMOC fingerprints (Boers, 2021; Ditlevsen and Ditlevsen, 2023; Hallali et al., 2025), and should not be seen as an "all-clear" signal. Instead, they highlight that small changes in methodological choices, such as window size, can change the conclusions from EWS analyses, which raises questions about the reliability of EWSs for abrupt transitions.

Significant increases in the PARCAD-N score under linear forcing suggest that recent AMOC changes were driven by an increase in a linear driver, consistent with prior studies (e.g., Boers, 2021; Ditlevsen and Ditlevsen, 2023; Hallali et al., 2025). However, the consistently low values of this indicator reveal no evidence of an imminent AMOC collapse. We further found no indication in PARCAD-N for a destabilization when the runoff forcing scenarios has been considered. Once again, these results can not be interpreted as an indication for a stable AMOC. In contrast to that, we found clear increases to high, considerable, and in part significant values of the N score in the second half of the 20th century, followed by a drop to lower values from 1980, which continued to decrease, despite being significant before the turn of the century. While this might be seen as a sign that the AMOC could have already passed a critical threshold around 1980, which aligns with previous results on significant AMOC changes in that time period (Zhu and Liu, 2020; Zhu et al., 2023; Coquereau et al., 2026), we simultaneously observe a maximal N score and a decrease in correlation. It is thus highly uncertain whether the parabolic approximations underlying the PARCAD-N score are reliable, which questions the validity of the apparent EWS observed here. Hence, a false warning cannot be ruled out. Low correlation values generally indicate a poor parabolic fit between all forcing time series, especially iCWG, and the AMOC fingerprint. Such low correlation might further be explained by the use of relatively short approximation intervals, as low correlation values for shorter intervals were also found for conceptual systems (see Figure 4E, F). Low correlation there, especially close to the diagonal of the matrices, i.e., as $a \to b$, indicate that approximately 100–150 data points are required for reliable polynomial fits. The analyzed AMOC fingerprint, however, only spans 150 years, which primarily allows for considerably shorter estimation intervals, which appear to be dominated by noise. This is in accordance with previous findings by Cotronei et al. (2026), where it has been shown that the variability of the AMOC fingerprint prevents reliable polynomial approximations. Our results further highlight the complexity gap between highly complex and multi-dimensional climate (sub-)systems, like the AMOC, and one-dimensional models providing the backbone of EWS analyses.

A recent study (Ritchie et al., 2021) suggests that the critical threshold of the AMOC, and other slow-onset tipping elements, might be temporarily exceeded ("overshot") without triggering an abrupt state transition under the current high rates of warming. This phenomenon is closely related to rate-induced tipping (Ashwin et al., 2012). It has been shown that an overshoot due to different timescales of a system and its control parameters typically leads to detection of CSD after the critical threshold has been passed (Ritchie et al., 2023; Radhakrishnan et al., 2025). Furthermore, it cannot be ruled out that random perturbations might lead to state transitions before the critical point of a system has been reached (noise-induced tipping), which cannot be captured by CSD-based EWSs. Alternative approaches (e.g., Ritchie et al., 2023; Huang et al., 2024) have been developed to foresee and predict rate- and noise-induced tipping. The approaches presented here are designed to detect stability changes prior to bifurcation-induced transitions and might not be readily applicable to systems undergoing rate-induced tipping. However, directly including non-linear forcing scenarios into our RMLA approach allows us to estimate the AMOC's sensitivity to a given control parameter, which, e.g., in the case of runoff forcing, changes on a faster timescale than the AMOC fingerprint.

To obtain reliable EWS prior to rate-induced transitions with the PARCAD methods, its assumptions, such as closeness of the AMOC fingerprint to an underlying stable branch of the system, should be fulfilled. PARCAD relies on multiple estimations of the bifurcation point and we expect significant high values in the N score to occur before a critical point in forcing has been reached. Late-onset tipping could therefore be reflected by a decreased N score once the bifurcation point has been passed. While such behavior has been observed for the AMOC with temperature forcing, we do not necessarily interpret this as an indication of having overshot a critical transition in the late 1970s, as low correlation coefficients indicate rather poor parabolic approximations.

Our analysis of multiple forcing scenarios via two complementary tools adds breadth to the current understanding of AMOC stability by demonstrating the sensitivity of EWSs to assumptions about forcing scenarios, response models, and evaluation criteria. Our results suggest that incorporating non-linear forcing scenarios and alternative approaches can provide a more nuanced perspective on possible tipping dynamics of the AMOC. This emphasizes the importance of methodological rigor and the need to account for the inherent complexity of the system. Moreover, we highlight that the robustness of EWS analyses is crucial for their interpretation, as it ensures the reliability and credibility of the results. It is thus imperative to avoid a selective presentation of only the most favorable results. Such "cherry-picking" can lead to biased conclusions and undermine the integrity of analyses. Finally, our findings underscore that multiple avenues of validation are required to draw reliable conclusions about the stability of potential TEs.

5.2 Limitations

While our methods represent a step forward, they are not without limitations. Similar to other commonly used EWS approaches, both RMLA and PARCAD rely on good model and polynomial fits, respectively, of the AMOC fingerprint, i.e., the assumed state variable, and forcing data, which may not always be achievable given the complexity of the system. However, the precise fit of a statistical model within the RMLA framework does not imply that the given model accurately describes the underlying system dynamics. To ensure reliable results within the PARCAD approach, the observed state, here the AMOC fingerprint, should remain close to its equilibrium state. Unfortunately, this cannot be easily verified for the highly complex dynamics of the AMOC. However, this is counter-indicated by the low correlation coefficients $PCC_{a,b}$ observed for both linear and non-linear forcing scenarios. The observed low correlation might further be attributed to the use of relatively short approximation intervals, whose lengths are constrained by the relatively short AMOC and forcing proxy time series. Moreover, PARCAD requires data with a relatively low signal-to-noise-ratio, which might be obtained by smoothing the data.

The integration of forcing time series, while still a simplification, allows us to focus on dominant drivers like temperature and Greenland meltwater runoff. However, our approaches do not capture the full range of complex and interacting processes that could contribute to an AMOC collapse, which are themselves affected by anthropogenic climate change (Stommel, 1961; Rahmstorf, 1995; Hawkins et al., 2011; Liu et al., 2017; Weijer et al., 2019; Gong et al., 2022). Additionally, the one-dimensional time series data, both describing the TE and its forcing, are assumed to accurately represent complex, spatially extended systems, which is certainly a simplification. The time series under investigation should further be suitable for EWS analyses: long enough to capture the dynamics on relevant time scales, spanning the time period of interest, without large data gaps and not dominated by noise. Unfortunately, such data is not always available and direct observations are often too short to observe relevant dynamics driving stability changes. For instance, suitable direct observations of AMOC strength are only available from 2004 (Smeed et al., 2014). Instead, it is common practice to use proxies ("fingerprints"), such as the AMOC fingerprint analysed here. While such SPG-based fingerprints are commonly used and they were found to be sensitive to stability changes (Menary et al., 2015; Sun et al., 2021; Swingedouw et al., 2022; Ben-Yami et al., 2023), their use as AMOC proxy is debated (Little et al., 2020; Zhu et al., 2023) and alternative proxies have been developed (e.g., Zhu and Liu, 2020; Zhu et al., 2023). Ben-Yami et al. (2024) highlight that uncertainties in such proxy datasets can lead to large uncertainties in the estimation of future tipping times and we cannot rule out that data uncertainties of the applied forcing data could lead to even greater uncertainties regarding the stability of the AMOC.

Effective freshwater flux is considered a realistic forcing parameter for the AMOC (Rahmstorf et al., 2005; Hofmann and Rahmstorf, 2009), but long-term measurements are unavailable. As a proxy, we used cumulative Greenland meltwater runoff (iCWG), which contributes to the effective freshwater flux, acknowledging that neither freshwater flux nor runoff scales linearly with temperature (Bamber et al., 2018; Trusel et al., 2018), and thus further motivating the integration of a freshwater driver. However, other contributors to the effective freshwater flux, such as Arctic freshwater input and changes in evaporation and precipitation have not been included here since observation-based time series suitable for our analysis are unavailable.

We further acknowledge that Northern Hemisphere mean near-surface temperatures (NH NST) only provide a simple proxy for global warming, which is more directly linked to freshwater changes in the North Atlantic than global mean temperature, but cannot fully represent the ongoing anthropogenic climate change or the complex interactions between (near-)surface temperatures and the AMOC. This highlights the need for more comprehensive datasets, more sophisticated analytical frameworks and approaches that integrate multiple interacting drivers. However, as also pointed out by Ben-Yami et al. (2024), such approaches, just like the ones presented here, require a careful consideration of modeling assumptions and data properties.

5.3 Future directions

Future research should focus on integrating multiple interacting forcing scenarios into EWS analyses to better capture the complexity of AMOC dynamics. This could involve combining temperature, freshwater flux, and sea ice dynamics into a unified framework. Additionally, the development of more robust statistical models that account for higher-dimensional dynamics could improve the reliability of EWSs. For example, extending the

RMLA method to include interacting drivers could yield valuable insights.

Another promising direction is the application of these methods to other potential climate tipping elements, such as the the Greenland Ice Sheet. The flexibility of the RMLA and PARCAD approaches makes them well-suited for analysing a wide range of systems, provided that appropriate system and forcing data are available. Furthermore, future studies could explore the estimation of tipping times using PARCAD or extend the RMLA framework by including alternative response functions and noise structures.

We note that these suggestions are currently still bound by the same limitations as those described in Section 5.2 above, especially those concerning observational datasets. It is thus paramount to ensure that the respective data provides a reliable, appropriate and representative approximation of the forcing and system state time series. This further calls for thorough investigations of such datasets, as they are essential for studies of climate TPs, which might be crossed due to the ongoing emission of anthropogenic greenhouse gases.

5.4 Broader implications

Finally, while our results highlight the limitations of EWSs for the AMOC, they also underscore the potential of these tools to provide valuable insights into the stability of complex climate (sub-)systems. Precursor signals like CSD-based EWSs, increased sensitivity, or the PARCAD-N score can indicate potential destabilization, but they are not guaranteed to capture the full dynamics of the system. This is especially the case for systems with high inter-annual variability or low signal-to-noise ratio. Future work should aim to bridge the gap between low-dimensional models, on which EWS analyses are based, and the high-dimensional reality of climate systems, ultimately improving our ability to predict and mitigate the impacts of tipping points in the Earth system.

Data availability statement

The AMOC fingerprint data analysed here are annual means of the fingerprint introduced by Ditlevsen and Ditlevsen (2023), which is available at https://doi.org/10.17894/ucph.9ef73d8c-b642-4b55-88bc-b38984d043b9. The CWG melt stack used to calculate iCWG forcing has been obtained from the provided source data to Trusel et al. (2018) (https://www.nature.com/articles/s41586-018-0752-4#Sec14). NH NST corresponds to the annual Northern hemisphere analysis time series ensemble mean from the HADCRUT5.0.2.0 data set (Morice et al., 2021) and can be found at the Met Office website https://www.metoffice.gov.uk/hadobs/hadcrut5/data/HadCRUT.5.0.2.0/download.html. The INLA.climate R package (Myrvoll-Nilsen et al., 2020) employed for the RMLA approach can be found at https://github.com/eirikmn/INLA.climate. The direct implementation of fGn within the INLA framework, used to compare RMLA model fits, has been adapted from Sørbye and Rue (2017) (https://doi.org/10.6084/m9.figshare.5134816). All R and Python code used for the RMLE and PARCAD analyses presented in this manuscript are available upon request.

Author contributions

CH: Conceptualization, Methodology, Writing – review & editing, Formal analysis, Writing – original draft, Investigation, Software, Visualization, Data curation, Validation. AC: Conceptualization, Methodology, Investigation, Data curation, Writing – review & editing, Writing – original draft, Formal analysis, Software. EM-N: Formal analysis, Writing – review & editing, Investigation, Data curation, Methodology, Software. NA: Writing – review & editing, Supervision, Conceptualization. MR: Writing – review & editing, Supervision, Methodology, Funding acquisition, Resources, Conceptualization, Project administration.

Funding

The author(s) declared that financial support was received for this work and/or its publication. This project has received funding from the European Union's Horizon 2020 research and innovation programme under the Marie Skodowska-Curie grant agreement no. 956170 (CriticalEarth). It has further been supported by the Research Council of Norway (project numbers 314570, 350036, and 332901), and the UiT Aurora Centre Program, UiT The Arctic University of Norway (2025).

Conflict of interest

The author(s) declared that this work was conducted in the absence of any commercial or financial relationships that could be construed as a potential conflict of interest.

Generative AI statement

The author(s) declared that Generative AI was not used in the creation of this manuscript.

Any alternative text (alt text) provided alongside figures in this article has been generated by Frontiers with the support of artificial intelligence and reasonable efforts have been made to ensure accuracy, including review by the authors wherever possible. If you identify any issues, please contact us.

Publisher's note

All claims expressed in this article are solely those of the authors and do not necessarily represent those of their affiliated organizations, or those of the publisher, the editors and the reviewers. Any product that may be evaluated in this article, or claim that may be made by its manufacturer, is not guaranteed or endorsed by the publisher.

Supplementary material

The Supplementary Material for this article can be found online at: https://www.frontiersin.org/articles/10.3389/fclim.2026.1826661/full#supplementary-material

References

Armstrong McKay, D. I., Staal, A., Abrams, J. F., Winkelmann, R., Sakschewski, B., Loriani, S., et al. (2022). Exceeding 1.5C global warming could trigger multiple climate tipping points. *Science* 377:eabn7950. doi: 10.1126/science.abn7950

Ashwin, P., Wieczorek, S., Vitolo, R., and Cox, P. (2012). Tipping points in open systems: bifurcation, noise-induced and rate-dependent examples in the climate system. *Philos. Trans.: Math. Phys. Eng. Sci.* 370, 1166–1184. doi: 10.1098/rsta.2011.0306

Bamber, J. L., Tedstone, A. J., King, M. D., Howat, I. M., Enderlin, E. M., van den Broeke, M. R., et al. (2018). Land ice freshwater budget of the Arctic and North Atlantic Oceans: 1. data, methods, and results. *J. Geophys. Res.: Oceans* 123, 1827–1837. doi: 10.1002/2017JC013605

Ben-Yami, M., Morr, A., Bathiany, S., and Boers, N. (2024). Uncertainties too large to predict tipping times of major Earth system components from historical data. *Sci. Adv.* 10:eadl4841. doi: 10.1126/sciadv.adl4841

Ben-Yami, M., Skiba, V., Bathiany, S., and Boers, N. (2023). Uncertainties in critical slowing down indicators of observation-based fingerprints of the Atlantic Overturning Circulation. *Nat. Commun.* 14:8344. doi: 10.1038/s41467-023-44046-9

Boers, N. (2018). Early-warning signals for Dansgaard-Oeschger events in a high-resolution ice core record. *Nat. Commun.* 9:2556. doi: 10.1038/s41467-018-04881-7

Boers, N. (2021). Observation-based early-warning signals for a collapse of the Atlantic Meridional Overturning Circulation. *Nat. Clim. Chang.* 11, 680–688. doi: 10.1038/s41558-021-01097-4

Boers, N., Ghil, M., and Rousseau, D.-D. (2018). Ocean circulation, ice shelf, and sea ice interactions explain Dansgaard–Oeschger cycles. *Proc. Nat. Acad. Sci. U. S. A.* 115, E11005–11014. doi: 10.1073/pnas.1802573115

Boers, N., Ghil, M., and Stocker, T. F. (2022). Theoretical and paleoclimatic evidence for abrupt transitions in the Earth system. *Environ. Res. Lett.* 17:093006. doi: 10.1088/1748-9326/ac8944

Boers, N., and Rypdal, M. (2021). Critical slowing down suggests that the western Greenland Ice Sheet is close to a tipping point. *Proc. Nat. Acad. Sci. U. S. A.* 118:e2024192118. doi: 10.1073/pnas.2024192118

Buckley, M. W., and Marshall, J. (2016). Observations, inferences, and mechanisms of the Atlantic Meridional Overturning Circulation: a review. *Rev. Geophys.* 54, 5–63. doi: 10.1002/2015RG000493

Caesar, L., Rahmstorf, S., Robinson, A., Feulner, G., and Saba, V. (2018). Observed fingerprint of a weakening Atlantic Ocean overturning circulation. *Nature* 556, 191–196. doi: 10.1038/s41586-018-0006-5

Coquereau, A., Sévellec, F., Huck, T., Hirschi, J. J.-M., and Jamet, Q. (2026). Past, present, and future variability of Atlantic meridional overturning circulation in CMIP6 ensembles. *Earth Syst. Dyn.* 17, 209–233. doi: 10.5194/esd-17-209-2026

Cotronei, A., Myrvoll-Nilsen, E., and Rypdal, M. (2026). Evaluating model uncertainty in critical threshold estimations from time series data: application to the Atlantic meridional Overturning Circulation. *Front. Clim.* 8:1761461. doi: 10.3389/fclim.2026.1761461

Dakos, V., Scheffer, M., van Nes, E. H., Brovkin, V., Petoukhov, V., and Held, H. (2008). Slowing down as an early warning signal for abrupt climate change. *Proc. Nat. Acad. Sci. U. S. A.* 105, 14308–14312. doi: 10.1073/pnas.0802430105

Ditlevsen, P., and Ditlevsen, S. (2023). Warning of a forthcoming collapse of the Atlantic meridional overturning circulation. *Nat. Commun.* 14:4254. doi: 10.1038/s41467-023-39810-w

Drijfhout, S. (2015). Competition between global warming and an abrupt collapse of the AMOC in Earth's energy imbalance. *Sci. Rep.* 5:14877. doi: 10.1038/srep14877

Drijfhout, S. S., Weber, S. L., and Van Der Swaluw, E. (2011). The stability of the MOC as diagnosed from model projections for pre-industrial, present and future climates. *Clim. Dyn.* 37, 1575–1586. doi: 10.1007/s00382-010-0930-z

Gong, X., Liu, H., Wang, F., and Heuz, C. (2022). Of Atlantic Meridional Overturning Circulation in the CMIP6 project. *Deep Sea Res. Part II: Top. Stud. Oceanogr.* 206:105193. doi: 10.1016/j.dsr2.2022.105193

Hallali, L., Myrvoll-Nilsen, E., and Franzke, C. L. E. (2025). Assessing AMOC stability using a Bayesian nested time-dependent autoregressive model. *Nonlin. Process. Geophys.* 32, 383–395. doi: 10.5194/npg-32-383-2025

Hawkins, E., Smith, R. S., Allison, L. C., Gregory, J. M., Woollings, T. J., Pohlmann, H., et al. (2011). Bistability of the Atlantic overturning circulation in a global climate model and links to ocean freshwater transport. *Geophys. Res. Lett.* 38:7208. doi: 10.1029/2011GL047208

Henry, L. G., McManus, J. F., Curry, W. B., Roberts, N. L., Piotrowski, A. M., and Keigwin, L. D. (2016). North Atlantic ocean circulation and abrupt climate change during the last glaciation. *Science* 353, 470–474. doi: 10.1126/science.aaf5529

Hofmann, M., and Rahmstorf, S. (2009). On the stability of the Atlantic meridional overturning circulation. *Proc. Nat. Acad. Sci. U. S. A.* 106, 20584–20589. doi: 10.1073/pnas.0909146106

Huang, Y., Bathiany, S., Ashwin, P., and Boers, N. (2024). Deep learning for predicting rate-induced tipping. *Nat. Mach. Intell.* 6, 1556–1565. doi: 10.1038/s42256-024-00937-0

Hummel, C., Boers, N., and Rypdal, M. (2025). Inconclusive early warning signals for Dansgaard-Oeschger events across Greenland ice cores. *Earth Syst. Dyn.* 16, 2035–2062. doi: 10.5194/esd-16-2035-2025

Ibrahim, J. G., Chen, M.-H., and Sinha, D. (2001). *Bayesian Survival Analysis. Springer Series in Statistics*. New York, NY: Springer. doi: 10.1007/978-1-4757-3447-8

Jackson, L. C., Kahana, R., Graham, T., Ringer, M. A., Woollings, T., Mecking, J. V., et al. (2015). Global and European climate impacts of a slowdown of the AMOC in a high resolution GCM. *Clim. Dyn.* 45, 3299–3316. doi: 10.1007/s00382-015-2540-2

Jackson, L. C., and Wood, R. A. (2020). Fingerprints for early detection of changes in the AMOC. *J. Clim.* 33, 7027–7044. doi: 10.1175/JCLI-D-20-0034.1

Kass, R. E., and Raftery, A. E. (1995). Bayes factors. *J. Am. Stat. Assoc.* 90, 773–795. doi: 10.1080/01621459.1995.10476572

Kindler, P., Guillevic, M., Baumgartner, M., Schwander, J., Landais, A., and Leuenberger, M. (2014). Temperature reconstruction from 10 to 120 kyr b2k from the NGRIP ice core. *Clim. Past* 10, 887–902. doi: 10.5194/cp-10-887-2014

Latif, M., Roeckner, E., Botzet, M., Esch, M., Haak, H., Hagemann, S., et al. (2004). Reconstructing, monitoring, and predicting multidecadal-scale changes in the North Atlantic Thermohaline circulation with sea surface temperature. *J. Clim.* 17, 1605–1614. doi: 10.1175/1520-0442(2004)017<1605:RMAPMC>2.0.CO;2

Lenton, T. M. (2011). Early warning of climate tipping points. *Nat. Clim. Chang.* 1, 201–209. doi: 10.1038/nclimate1143

Lenton, T. M., Held, H., Kriegler, E., Hall, J. W., Lucht, W., Rahmstorf, S., et al. (2008). Tipping elements in the Earth's climate system. *Proc. Nat. Acad. Sci. U. S. A.* 105, 1786–1793. doi: 10.1073/pnas.0705414105

Little, C. M., Zhao, M., and Buckley, M. W. (2020). Do surface temperature indices reflect centennial-timescale trends in Atlantic Meridional overturning circulation strength? *Geophys Res Lett.* 47:e2020GL090888. doi: 10.1029/2020GL090888

Liu, W., Fedorov, A. V., Xie, S.-P., and Hu, S. (2020). Climate impacts of a weakened Atlantic Meridional Overturning Circulation in a warming climate. *Sci. Adv.* 6:eaaz4876. doi: 10.1126/sciadv.aaz4876

Liu, W., Liu, Z., and Brady, E. C. (2014). Why is the AMOC monostable in coupled general circulation models? *J. Clim.* 27, 2427–2443. doi: 10.1175/JCLI-D-13-00264.1

Liu, W., Xie, S.-P., Liu, Z., and Zhu, J. (2017). Overlooked possibility of a collapsed Atlantic Meridional Overturning Circulation in warming climate. *Sci. Adv.* 3:e1601666. doi: 10.1126/sciadv.1601666

Lynch-Stieglitz, J. (2017). The Atlantic Meridional Overturning circulation and abrupt climate change. *Annu. Rev. Mar. Sci.* 9, 83–104. doi: 10.1146/annurev-marine-010816-060415

Manabe, S., and Stouffer, R. J. (1988). Two stable equilibria of a coupled ocean-atmosphere model. *J. Clim.* 1, 841–866.

Mandelbrot, B. B., and Van Ness, J. W. (1968). Fractional Brownian motions, fractional noises and applications. *SIAM Rev.* 10, 422–437. doi: 10.1137/1010093

Mecking, J., Drijfhout, S., Jackson, L., and Andrews, M. (2017). The effect of model bias on Atlantic freshwater transport and implications for AMOC bi-stability. *Tellus A: Dyn. Meteorol. Oceanogr.* 69:1299910. doi: 10.1080/16000870.2017.1299910

Mei, Y., He, W., Xie, X., Wan, S., and Gu, B. (2023). Increasing long-term memory as an early warning signal for a critical transition. *J. Clim.* 37, 487–504. doi: 10.1175/JCLI-D-22-0263.1

Menary, M. B., Hodson, D. L. R., Robson, J. I., Sutton, R. T., and Wood, R. A. (2015). A mechanism of internal decadal atlantic ocean variability in a high-resolution coupled climate model. *J. Clim.* 28, 7764–7785. doi: 10.1175/JCLI-D-15-0106.1

Michel, S. L. L., Swingedouw, D., Ortega, P., Gastineau, G., Mignot, J., McCarthy, G., et al. (2022). Early warning signal for a tipping point suggested by a millennial Atlantic Multidecadal Variability reconstruction. *Nat. Commun.* 13:5176. doi: 10.1038/s41467-022-32704-3

Morice, C. P., Kennedy, J. J., Rayner, N. A., Winn, J. P., Hogan, E., Killick, R. E., et al. (2021). An updated assessment of near-surface temperature change from 1850: the HadCRUT5 data set. *J. Geophys. Res.: Atmos.* 126:e2019JD032361. doi: 10.1029/2019JD032361

Myrvoll-Nilsen, E., Hallali, L., and Rypdal, M. (2025). Bayesian analysis of early warning signals using a time-dependent model. *Earth Syst. Dyn.* 16, 1539–1556. doi: 10.5194/esd-16-1539-2025

Myrvoll-Nilsen, E., Srbye, S. H., Fredriksen, H.-B., Rue, H., and Rypdal, M. (2020). Statistical estimation of global surface temperature response to forcing under the assumption of temporal scaling. *Earth Syst. Dyn.* 11, 329–345. doi: 10.5194/esd-11-329-2020

Oh, J.-H., Kug, J.-S., Shin, Y., Geng, X., Wang, S., Jin, F.-F., et al. (2025). Noise-induced tipping of Atlantic Meridional Overturning Circulation under climate mitigation scenarios. *Nat. Commun.* 16:11515. doi: 10.1038/s41467-025-66494-1

Pettit, L. I. (1990). The conditional predictive ordinate for the normal distribution. *J. R. Stat. Soc. Ser. B (Methodol.)* 52, 175–184. doi: 10.1111/j.2517-6161.1990.tb01780.x

Radhakrishnan, R., Pavithran, I., Livina, V., Kurths, J., and Sujith, R. I. (2025). Early warnings are too late when parameters change rapidly. *Sci. Rep.* 15:20256. doi: 10.1038/s41598-025-06525-5

Rahmstorf, S. (1995). Bifurcations of the Atlantic thermohaline circulation in response to changes in the hydrological cycle. *Nature* 378, 145–149. doi: 10.1038/378145a0

Rahmstorf, S. (2002). Ocean circulation and climate during the past 120,000 years. *Nature* 419, 207–214. doi: 10.1038/nature01090

Rahmstorf, S., Box, J. E., Feulner, G., Mann, M. E., Robinson, A., Rutherford, S., et al. (2015). Exceptional twentieth-century slowdown in Atlantic Ocean overturning circulation. *Nat. Clim. Change* 5, 475–480. doi: 10.1038/nclimate2554

Rahmstorf, S., Crucifix, M., Ganopolski, A., Goosse, H., Kamenkovich, I., Knutti, R., et al. (2005). Thermohaline circulation hysteresis: a model intercomparison. *Geophys. Res. Lett.* 32:3655. doi: 10.1029/2005GL023655

Rayner, N. A., Parker, D. E., Horton, E. B., Folland, C. K., Alexander, L. V., Rowell, D. P., et al. (2003). Global analyses of sea surface temperature, sea ice, and night marine air temperature since the late nineteenth century. *J. Geophys. Res.: Atmos.* 108:2670. doi: 10.1029/2002JD002670

Rietkerk, M., Skiba, V., Weinans, E., Hébert, R., and Laepple, T. (2025). Ambiguity of early warning signals for climate tipping points. *Nat. Clim. Chang.* 15, 479–488. doi: 10.1038/s41558-025-02328-8

Ritchie, P. D. L., Alkhayuon, H., Cox, P. M., and Wieczorek, S. (2023). Rate-induced tipping in natural and human systems. *Earth Syst. Dyn.* 14, 669–683. doi: 10.5194/esd-14-669-2023

Ritchie, P. D. L., Clarke, J. J., Cox, P. M., and Huntingford, C. (2021). Overshooting tipping point thresholds in a changing climate. *Nature* 592, 517–523. doi: 10.1038/s41586-021-03263-2

Robert, C., and Casella, G. (1999). *Monte Carlo Statistical Methods. Springer Texts in Statistics, 1st Edn.* New York, NY: Springer New York. doi: 10.1007/978-1-4757-3071-5

Roberts, C. D., Garry, F. K., and Jackson, L. C. (2013). A multimodel study of sea surface temperature and subsurface density fingerprints of the atlantic meridional overturning circulation. *J. Clim.* 26, 9155–9174. doi: 10.1175/JCLI-D-12-00762.1

Romanou, A., Rind, D., Jonas, J., Miller, R., Kelley, M., Russell, G., et al. (2023). Stochastic bifurcation of the North Atlantic circulation under a midrange future climate scenario with the NASA-GISS ModelE. *J. Clim.* 36, 6141–6161. doi: 10.1175/JCLI-D-22-0536.1

Rue, H., Martino, S., and Chopin, N. (2009). Approximate Bayesian inference for latent Gaussian models by using integrated nested Laplace approximations. *J. R. Stat. Soc.: Ser. B (Stat. Method.)* 71, 319–392. doi: 10.1111/j.1467-9868.2008.00700.x

Rue, H., Riebler, A., Sørbye, S. H., Illian, J. B., Simpson, D. P., and Lindgren, F. K. (2017). Bayesian computing with INLA: a review. *Annu. Rev. Stat. Appl.* 4, 395–421. doi: 10.1146/annurev-statistics-060116-054045

Rypdal, M. (2016). Early-warning signals for the onsets of Greenland Interstadials and the Younger Dryas–Preboreal transition. *J. Clim.* 29, 4047–4056. doi: 10.1175/JCLI-D-15-0828.1

Rypdal, M., Fredriksen, H.-B., Myrvoll-Nilsen, E., Rypdal, K., and Srbye, S. H. (2018). Emergent scale invariance and climate sensitivity. *Climate* 6:93. doi: 10.3390/cli6040093

Rypdal, M., and Rypdal, K. (2014). Long-memory effects in linear response models of earth's temperature and implications for future global warming. *J. Clim.* 27, 5240–5258. doi: 10.1175/JCLI-D-13-00296.1

Scheffer, M., Bascompte, J., Brock, W. A., Brovkin, V., Carpenter, S. R., Dakos, V., et al. (2009). Early-warning signals for critical transitions. *Nature* 461, 53–59. doi: 10.1038/nature08227

Schwarz, G. (1978). Estimating the dimension of a model. *Ann. Stat.* 6, 461–464. doi: 10.1214/aos/1176344136

Smeed, D. A., McCarthy, G. D., Cunningham, S. A., Frajka-Williams, E., Rayner, D., Johns, W. E., et al. (2014). Observed decline of the Atlantic meridional overturning circulation 2004–2012. *Ocean Sci.* 10, 29–38. doi: 10.5194/os-10-29-2014

Sørbye, S. H., and Rue, H. (2017). Dataset for: fractional Gaussian noise: prior specification and model comparison. Wiley. Dataset. doi: 10.6084/m9.figshare.5134816.v1

Sørbye, S. H., and Rue, H. (2018). Fractional Gaussian noise: prior specification and model comparison. *Environmetrics* 29:e2457. doi: 10.1002/env.2457

Sørbye, S. H., and Rue, H. (2019). An approximate fractional gaussian noise model with $\mathcal{O}\Leftarrow\backslash\Rightarrow$ computational cost. *Stat. Comput.* 29, 821–833. doi: 10.1007/s11222-018-9843-1

Spiegelhalter, D. J., Best, N. G., Carlin, B. P., and Van Der Linde, A. (2002). Bayesian measures of model complexity and fit. *J. R. Stat. Soc.: Ser. B (Stat. Methodol.y)* 64, 583–639. doi: 10.1111/1467-9868.00353

Stommel, H. (1961). Thermohaline convection with two stable regimes of flow. *Tellus* 13, 224–230. doi: 10.1111/j.2153-3490.1961.tb00079.x

Stouffer, R. J., Yin, J., Gregory, J. M., Dixon, K. W., Spelman, M. J., Hurlin, W., et al. (2006). Investigating the causes of the response of the thermohaline circulation to past and future climate changes. *J. Clim.* 19, 1365–1387. doi: 10.1175/JCLI3689.1

Strogatz, S. H. (2018). *Nonlinear Dynamics and Chaos: With Applications to Physics, Biology, Chemistry, and Engineering, 2nd Edn.* Boca Raton, FL: CRC Press. doi: 10.1201/9780429399640

Sun, J., Latif, M., and Park, W. (2021). Subpolar GyreAMOC atmosphere interactions on multidecadal timescales in a version of the Kiel Climate Model. *J. Clim.* 34, 6583–6602. doi: 10.5194/egusphere-egu21-4608

Swingedouw, D., Houssais, M.-N., Herbaut, C., Blaizot, A.-C., Devilliers, M., and Deshayes, J. (2022). AMOC recent and future trends: a crucial role for oceanic resolution and greenland melting? *Front. Clim.* 4:838310. doi: 10.3389/fclim.2022.838310

Trusel, L. D., Das, S. B., Osman, M. B., Evans, M. J., Smith, B. E., Fettweis, X., et al. (2018). Nonlinear rise in Greenland runoff in response to post-industrial Arctic warming. *Nature* 564, 104–108. doi: 10.1038/s41586-018-0752-4

Valdes, P. (2011). Built for stability. *Nat. Geosci.* 4, 414–416. doi: 10.1038/ngeo1200

van Westen, R. M., Kliphuis, M., and Dijkstra, H. A. (2024). Physics-based early warning signal shows that AMOC is on tipping course. *Sci. Adv.* 10:eadk1189. doi: 10.1126/sciadv.adk1189

Wagner, T. J. W., and Eisenman, I. (2015). False alarms: how early warning signals falsely predict abrupt sea ice loss. *Geophys. Res. Lett.* 42, 10333–10341. doi: 10.1002/2015GL066297

Watanabe, S., and Opper, M. (2010). Asymptotic equivalence of Bayes cross validation and widely applicable information criterion in singular learning theory. *J. Mach. Learn. Res.* 11:3571–3594. doi: 10.5555/1756006.1953045

Weijer, W., Cheng, W., Drijfhout, S. S., Fedorov, A. V., Hu, A., Jackson, L. C., et al. (2019). Stability of the Atlantic Meridional overturning circulation: a review and synthesis. *J. Geophys. Res.: Oceans* 124, 5336–5375. doi: 10.1029/2019JC015083

Witelski, T., and Bowen, M. (2015). "Fast/slow dynamical systems," in *Methods of Mathematical Modelling*. Springer Undergraduate Mathematics Series. Cham: Springer. doi: 10.1007/978-3-319-23042-9_10

Wunderling, N., von der Heydt, A. S., Aksenov, Y., Barker, S., Bastiaansen, R., Brovkin, V., et al. (2024). Climate tipping point interactions and cascades: a review. *Earth Syst. Dyn.* 15, 41–74. doi: 10.5194/esd-15-41-2024

Wunderling, N., Winkelmann, R., Rockstrm, J., Loriani, S., Armstrong McKay, D. I., Ritchie, P. D. L., et al. (2023). Global warming overshoots increase risks of climate tipping cascades in a network model. *Nat. Clim. Change* 13, 75–82. doi: 10.1038/s41558-022-01545-9

Zhu, C., and Liu, Z. (2020). Weakening Atlantic overturning circulation causes South Atlantic salinity pile-up. *Nat. Clim. Chang.* 10, 998–1003. doi: 10.1038/s41558-020-0897-7

Zhu, C., Liu, Z., Zhang, S., and Wu, L. (2023). Likely accelerated weakening of Atlantic overturning circulation emerges in optimal salinity fingerprint. *Nat. Commun.* 14:1245. doi: 10.1038/s41467-023-36288-4

Zimmerman, C. C., Wagner, T. J. W., Maroon, E. A., and McNamara, D. E. (2025). Slowed response of Atlantic Meridional overturning circulation not a robust signal of collapse. *Geophys. Res. Lett.* 52:e2024GL112415. doi: 10.1029/2024GL112415